Introduction, Characterization and Efficiency Optimization of an $Al_xGa_{1-x}As$ / $Al_xIn_{1-x}As$ Heterojunction Solar cell with $Ga_xIn_{1-x}As$ Back Surface Field (BSF) Layer Using ADEPT/F

A Dissertation Submitted in Partial Fulfilment of Requirement for the Degree of Bachelor of Science in Electrical and Electronic Engineering

Submitted by

K.A.S.M. Ehteshamul Haque

Mohammad Tanvirul Ferdaous

Tahmid Nahian Bin Quddus

Under The Supervision Of

DR. MD. ASHRAFUL HOQUE

PROFESSOR

DEPARTMENT OF ELECTRICAL AND ELECTRONIC ENGINEERING (EEE)

ISLAMIC UNIVERSITY OF TECHNOLOGY (IUT)

THE ORGANIZATION OF THE ISLAMIC COOPERATION (OIC)

GAZIPUR-1704, DHAKA, BANGLADESH

Introduction, Characterization and Efficiency Optimization of an $Al_xGa_{1-x}As$ / $Al_xIn_{1-x}As$ Heterojunction Solar Cell with $Ga_xIn_{1-x}As$ Back Surface Field (BSF) Layer Using ADEPT/F

A Thesis Presented to
The Academic Faculty

By

K.A.S.M. Ehteshamul Haque (Student ID: 082422)

Mohammad Tanvirul Ferdaous (Student ID: 082449)

Tahmid Nahian Bin Quddus (Student ID: 082457)

In Partial Fulfilment of Requirement for the Degree of Bachelor of Science in Electrical and Electronic Engineering

Approved By

PROF. DR. MD. ASHRAFUL HOQUE
DEPARTMENT OF ELECTRICAL AND ELECTRONIC ENGINEERING (EEE)
ISLAMIC UNIVERSITY OF TECHNOLOGY (IUT)

October, 2012

Table of Contents

Chapter 1- introduction

Chapter 2- The Initial Design

Chapter 3- Optimization of Device Parameters

Chapter 4- Optimization of Alloy Composition

Chapter 5- Practical Solutions for Fabrication Purpose

Chapter 6- Summary

List of Figures

List of Tables

Introduction, Characterization and Efficiency Optimization of an $Al_xGa_{1-x}As$ / $Al_xIn_{1-x}As$ Heterojunction Solar cell with $Ga_xIn_{1-x}As$ Back Surface Field (BSF) Layer Using ADEPT/F

Abstract

Energy conversion efficiency is a major issue for photovoltaic cells today. Researchers are continuously trying to improve the efficiency level of photovoltaic devices by introducing new materials and advanced concepts. The target is to reach a high efficiency level within affordable cost, which will lead to a mass generation of electricity using photovoltaic devices.

In this work, a III-V heterojunction solar cell has been introduced and characterized, which uses an $Al_xGa_{1-x}As/Al_xIn_{1-x}As$ heterojunction as the working p-n junction. ADEPT/F, a 1D simulation software, was used throughout the whole work for the simulation of light J-V characteristics for different designs. Energy conversion efficiency for each design was calculated from its corresponding light J-V characteristics curve. An illumination level of 1000 W/m^2 (AM1.5G standard) and a concentration level of 1 sun was considered for all the simulations in the work. The photovoltaic cell has an n-on-p structure, where the n-type $Al_{0.7}Ga_{0.3}As$ (x=0.7) layer acts as an emitter, and the p-type $Al_{0.48}In_{0.52}As$ (x=0.48) layer serves as the base (absorber). The base thickness was kept at 10 µm in the first simulation, and an energy conversion efficiency of 6.78% was obtained. Then, a lightly doped third layer (p-type) of $Ga_{0.67}In_{0.33}As$ was introduced (in contact with the base layer). This resulted in an efficiency of 15.3%, which was further increased to 16.79% after allowing a very high doping level (1×10^{19} cm^{-3}) in the $Ga_{0.67}In_{0.33}As$ layer. Germanium (Ge) substrate (p-doped) was used for the structure.

Afterwards, efficiency variation with change in device parameters (layer thickness and doping concentration) was investigated for the device. Variation in efficiency was plotted against a particular changing parameter, keeping every other parameter fixed at some default value. After analysing the variation curves, two optimized designs were proposed, which yield 19.57% and 20.56% efficiency, respectively.

In the later part of the work, variation in energy conversion efficiency was studied by changing the alloy composition at different layers of the device. Simulations were done for different combinations of alloy composition at device layers. The study was conducted by analyzing the efficiency values resulting for different combinations. The best results were obtained for x= 0.9, 0.48 and 0.9 in the top, middle and

bottom layer, respectively. For optimized values of layer thickness and doping concentration at different layers, this particular combination of alloy composition yielded an efficiency of 21.39%.

This particular design for the device had some drawbacks in practical fabrication. These drawbacks were addressed with appropriate solutions, and a number of changes were brought in the highest efficiency design. The modified design, which is fully feasible for fabrication, yields an efficiency of 17.03%.

Considering the high fabrication cost of III-V solar cells, a thin film solar cell design was proposed, which is only 2 μm thick (excluding the substrate thickness), and yields an efficiency of 12.16%. This efficiency was raised to 13.84% by using InP substrate, instead of Ge.

Acknowledgements

We are grateful to our thesis supervisor, Dr. Md. Ashraful Hoque, for his continuous guidance and motivation in completing our thesis. His constant demand for making the work more and more elaborate finally resulted in satisfactory outcomes. We would like to thank Khairul Anam, final year undergraduate student of the Department of Electrical and Electronics Engineering, Islamic University of Technology, for providing us with necessary information about heterojunction solar cells. We are also thankful to Shah Mohammad Bahauddin, final year undergraduate student of the Department of Applied Physics, Electronics and Communication Engineering, University of Dhaka, for offering us a helpful introduction to ADEPT/F.

Symbols & Abbreviations

I	Current (A)
I_L	Photocurrent (A)
I_F	Forward current (A)
I_S	Saturation current (A)
n	Ideality factor
k	Boltzmann constant (JK^{-1})
T	Absolute temperature (K)
q	Charge of an electron (C)
I_{sc}	Short-circuit current (A)
V_{oc}	Open-circuit voltage (V)
P_m	Maximum output power (W)
V_m	Voltage at maximum power point (V)
I_m	Current at maximum power point (A)
FF	Fill Factor
V_{ocn}	Normalized open-circuit voltage (V)
η	Energy conversion efficiency (%)
E	Solar irradiance (W/cm^2)
A	Area of the solar cell (cm^2)
J_{sc}	Short-circuit current density (A/cm^2)

Chapter 1- Introduction

1.9 Solar Cells

1.9.1 History

Solar cells are semiconductor devices which convert incident light into electricity by the absorption of photons and subsequent generation of electron-hole pairs. This effect of electricity generation from light absorption, which is known as the photovoltaic effect, was first observed by the French physicist A. E. Becquerel in 1839 [1]. The first solid-state photovoltaic cell was built many years later, by Charles Fritts, in 1883. He coated Selenium (Se) with an extremely thin layer of gold to form the junction. The photovoltaic device was less than 1% efficient [2]. The first practical photovoltaic cell was developed in 1954 at Bell Laboratories [3] by the three scientists- Daryl Chapin, Calvin Souther Fuller and Gerald Pearson. They used a diffused Silicon p-n junction that achieved 6% efficiency.

At present, solar cells are built with many different technologies, and the efficiency level that these devices can achieve is pretty good. In today's world, we have bulk Si solar cells, we have thin film solar cells fabricated from Si or CdTe, we have dye-sensitized solar cells, and so on. There are even more advanced concept solar cells like Quantum Dot (QD) solar cells, hot carrier solar cells etc. Today, solar cells are used for mass generation of electricity. The added advantage of solar power plants is that they require minimum maintenance, and the input energy is clean and free.

1.9.2 Principle of Operation

Figure 1.1 presents a simplified diagram [4] of a solar cell that utilizes a single p-n junction. With no voltage applied to this junction, an electric field exists in the depletion region of the p-n junction. For simplicity, we consider that a resistive load is connected with the device. Now, photons incident on the device can create electron-hole pairs in the space-charge region, which are forcibly swept out of the depletion region by the built-in electric field, as the depletion region must be depleted of free charges. This swept out carriers produce a photocurrent I_L, in the reverse-bias direction for the p-n junction. Now, the photocurrent I_L produces a voltage drop across the resistive load, which forward biases the p-n junction. This forward bias produces a forward current, I_F, in the forward-bias direction for the p-n junction. The net current, I, in the reverse bias direction for the p-n junction, is given by equation (1).

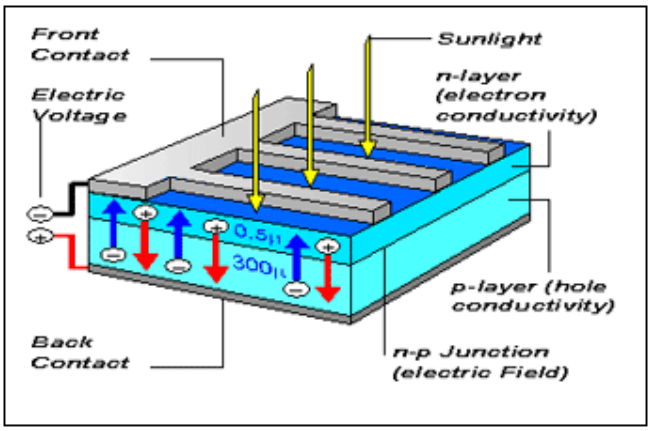

Fig. 1.1 Schematic diagram of a simplified back contact solar cell (image courtesy: ECN, the Netherlands).

$$I = I_L - I_F = I_L - I_S\,[exp\,(qV / nkT) - 1] \qquad (1)$$

Where,

n = Ideality factor (taken as 1)

k = Boltzmann constant

T = Temperature in K

q = charge of an electron

I_S = saturation current

1.9.3 Important Quantities

Now, there are two quantities of practical interest, the short-circuit current (I_{sc}) and the open-circuit voltage (V_{oc}). The short-circuit condition occurs when the resistive load is zero, so that V= 0. In this case, I_F is zero, and the short-circuit current, I_{sc}, is given by equation (2).

$$I_{sc} = I_L \qquad (2)$$

Open-circuit condition occurs when the load resistance is infinity. The net current is zero in this case, which finally gives the expression of the open-circuit voltage, V_{oc}, as shown in equation (3).

$$V_{oc} = (nkT / q)\,ln\,(1 + (I_L / I_S)) \qquad (3)$$

It is to be noted that at both short-circuit and open-circuit condition, the power output of a solar cell is zero. Actually, there is a maximum power point on the I-V characteristics graph of a solar cell where $\frac{dP}{dV} = 0$ (P is the output power). This point is called the maximum power point. The maximum output power, P_m, is given by,

$$P_m = V_m I_m \qquad (4)$$

Where,

V_m = Voltage at Maximum Power Point

I_m = Current at Maximum Power Point

Now, a quantity, termed as 'Fill Factor', is used to measure the 'squareness' of the I-V curve of a solar cell. This is the ratio of the maximum output power, P_m, to the product of short-circuit current (I_{sc}) and the open-circuit voltage (V_{oc}). Fill factor is commonly abbreviated as FF. A higher FF is desirable, since it increases the maximum output power.

The theoretical FF from a solar cell can be determined by differentiating the power from a solar cell with respect to the voltage and finding the voltage value for which the derivative equals to zero. This is the voltage corresponding to the maximum power point, which is denoted by V_m. An equation involving V_m is given in (5).

$$V_m = V_{oc} - [(nkT / q) \times [\ln (qV_m / nkT) + 1] \qquad (5)$$

Solving equation (5) by iteration gives the value of V_m. Now, determining the value of I_m requires the knowledge of I_L and I_S. So, this method does not give a closed form solution for determining the maximum output power P_m, the knowledge of which is required for determining FF. So, for all the simulations in our work, we have used the formula [5] given by equation (6) for the calculation of FF.

$$FF = \frac{Vocn - \ln(Vocn + 0.72)}{Vocn + 1} \qquad (6)$$

Where,

$$Vocn = \left(\frac{q}{nkT}\right) Voc \qquad (7)$$

Here,

V_{oc} = Open-circuit voltage (in Volt)

n= Ideality factor

q= Charge of an electron = 1.6×10^{-19} Coulomb

k= Boltzmann constant

T= Temperature in K

For all the simulations, we have considered n=1, and T = 300K.

The energy conversion efficiency of a solar cell, η, is given in (8).

$$\eta = \frac{Voc \times Isc \times FF}{E \times A} \times 100\% \qquad (8)$$

Here,

V_{oc} = Open-circuit voltage (in Volts)

I_{sc} = Short-circuit current (in Amperes)

FF = Fill Factor

E = Solar irradiance (in W/cm^2)

A= Area of the solar cell (in cm^2)

Now, I_{sc} /A can be termed as J_{sc}, which is the short-circuit current density (in A/cm^2). So, equation (8) can be rewritten as,

$$\eta = \frac{Voc \times Jsc \times FF}{E} \times 100\% \qquad (9)$$

Where,

J_{sc} = Short-circuit current density (in A/cm^2)

We are considering the use of the solar cell for terrestrial applications. So, to account for the incident sunlight, AM1.5G illumination was considered in the simulation code, as this is the standard terrestrial illumination. According to this, the solar irradiance, E, is taken to be 1000 W/m^2, or, 0.1 W/cm^2. It was also considered that the device is working under 1 sun i.e. no concentrator is used.

Using Equation (9), the energy conversion efficiency was calculated.

1.10 Heterojunction Solar Cells

A heterojunction is a p-n junction formed between two different semiconducting materials. Heterojunctions have got numerous applications in optoelectronic devices [6]. Heterojunction solar cells generally employ a p-n or p-i-n structure. In the simplified p-n structure, one material essentially works as an absorber, while the other can be a window layer, or another absorber [7]. The absorber is the functioning layer for optical absorption and generation of electron-hole pairs. The window layer is usually

a high bandgap material which is highly transparent to light, so that it can allow almost all the incident photons to reach the absorber.

Heterojunction devices have an inherent advantage over homojunction devices, which require materials that can be doped both p- and n-type. Many semiconducting materials can be doped either p-type or n-type, but not the both. Heterojunctions do not suffer from this limitation. So, many promising materials with good optical absorption capabilities can be investigated to produce optimal cells [8].

Again, a high-bandgap window layer reduces the cell's series resistance, and improves the output voltage [8]. It also helps to reduce recombination of minority carriers at the metal-semiconductor interface around the contacts [9].

For solar cells and other optoelectronic components, it is not sufficient to choose materials with suitable bandgap values and bring them to form a junction. It is also important to make sure that the chosen materials form a junction such that the interface is as much free of energy states in the forbidden band as possible, in order to prevent additional recombination of carriers and carrier trapping [9]. Material combinations satisfying such conditions are not very common. However, many combinations of III-V compounds, especially the ternary compounds based on GaAs, satisfy these criteria to large extents [9].

1.11 Silicon Alloys or III-V Materials – which one is a better choice for Heterojunctions?

Heterojunction solar cells involving Si and Si alloys have been thoroughly investigated [10]. But from a fundamental standpoint, Si is not a very good choice. Its bandgap is lower than the optimum bandgap required for achieving the highest level of efficiency. For terrestrial applications, the optimum bandgap of the absorber should be around 1.4 eV [11], while Si has an indirect bandgap of 1.12 eV. Besides this, Si has low optical absorption coefficient, compared to the high optical-absorption-compounds [12].

Now-a-days, III-V compounds have gained considerable interest as constituents of both single-junction and multijunction solar cells. The special advantage that these materials offer is their wide range of variation in bandgaps [13]. Besides this, they have got high optical absorption properties, along with high electron mobility and high minority carrier lifetime. They also provide numerous options for proper lattice matching between the heterojunction materials. So, photovoltaic cells fabricated from III-V compounds typically provide high output current and high efficiency. III-V ternary and quaternary alloys can offer yet

more flexibility, as their bandgaps and other properties can be finely tuned by changing the alloy composition.

1.12 III-V Compounds as Photovoltaic Materials

III-V semiconductors typically have the Zincblende crystal structure (except for the Nitrides), with a lattice constant varying in the range of 5.4 to 6.2 Å, depending on the material [14]. Along with the binary compounds, there are also ternary and quaternary compounds available. Among all the III-V compounds, the most widely used one for solar cells and many other applications is GaAs, due to its optimum direct bandgap (1.42 eV). Besides this, GaAs has got high electron mobility (8500 cm^2/ V-s), which makes it attractive for all types of solid-state devices. Single-junction solar cells fabricated from GaAs have achieved efficiency values as high as 28% [15]. Another promising III-V binary compound for the base layer of a solar cell is InP, which has an energy gap of 1.344 eV. Solar cells fabricated with monocrystalline InP have resulted in efficiencies around 22% [15]. Other compounds like $Al_xGa_{1-x}As$, $Ga_xIn_{1-x}As$, $Ga_xIn_{1-x}P$ and $Al_xGa_{1-x}As_yP_{1-y}$ have been frequently used in multijunction solar cells [12, 16]. High bandgap materials like GaP (E_g=2.26 eV) and AlAs (E_g=2.16 eV) have been utilized as the window layer of heterojunction solar cells [13].

The III-V Nitrides typically have Wurtzite lattice structure (except for BN), and they can provide a very wide range of bandgap variation. Application of ternary III-V Nitrides, such as $Al_xGa_{1-x}N$, has been investigated for multijunction cells in recent years [17].

1.13 Drawback of III-V Solar Cells

The problem associated with III-V solar cells is that these cells are very expensive, compared to the commonly used terrestrial solar cell technologies [18]. This is mainly due to the high fabrication cost of III-V materials, along with the unavailability of necessary fabrication technology in few cases. So, the use of III-V solar cells is still limited to space applications, where the efficiency is prioritized over the cost [19, 20]. Utilization of such solar cells for terrestrial applications requires reduction of materials processing and fabrication costs. Another way to address this problem is to use concentrators with solar cells. Concentrated solar cells can give up to 2000 times the power output of a solar cell working under 1 sun, depending on the concentration level. Though concentrators are very expensive, they can offer a good trade-off between the PV system cost and the achievable high efficiency [21].

1.14 About the Software

All the simulations conducted for this work were done by ADEPT/F [22]. It is a 1D simulation tool, which was developed by Jeff Gray and Michael McLennan from Purdue University, in 2008. This software can simulate the electrical characteristics of heterostructured semiconductor devices. It solves Poisson's equation coupled with the hole and electron continuity equations in one spatial dimension in compositionally non-uniform semiconductors. It was originally written to model solar cells fabricated from a wide variety of materials. Using this software, dark I-V characteristics, light I-V characteristics and spectral response of solar cells (or any other two-terminal device) can be computed. Plots of many internal parameters, such as carrier density, carrier velocity, electric field, etc. can be plotted at any operating point.

While working with this software, values of required material parameters (band gap, mobility, thickness, doping level etc.) are given as inputs by the user. Devices fabricated from any material, for which these parameters are known, can be modeled by the software.

1.15 Research Outlines

In our work, we have introduced, characterized and optimized a novel III-V heterojunction solar cell using ADEPT/F simulator that incorporates an $Al_xGa_{1-x}As$/ $Al_xIn_{1-x}As$ heterojunction. Here, the $Al_xIn_{1-x}As$ layer functions as the active (absorber) layer of the cell. A highly doped bottom layer of $Ga_xIn_{1-x}As$ was also introduced in the design, which works as a Back Surface Field (BSF) layer. Ge substrate is used for the structure. Optimization was done for the device parameters such as layer thickness and doping concentration. Alloy composition of the ternary compounds was also optimized for higher efficiency. The best design, which yields 21.4% efficiency, suffers from some basic difficulties in fabrication. In order to solve this, the issue of critical layer thickness with lattice mismatch was addressed carefully, and the revised design achieved 17.03% efficiency. A cost-effective thin film solar cell design was also proposed in the end.

1.16 Novelty in the Work

The base layer material, $Al_xIn_{1-x}As$, has been employed in the past in HEMT [23] and quantum cascade lasers [24]. This III-V compound has very recently gained attention as the constituent of homojunction solar cells [25, 26]. Till now, there is no evidence of heterojunction solar cells fabricated using $Al_xGa_{1-x}As$ / $Al_xIn_{1-x}As$ heterojunction. This work theoretically analyses the outcomes of applying this heterojunction in solar cells, along with the fabrication issues, discussed at the end of the work.

Chapter 2- The Initial Design

2.2 Choice of Materials

2.2.1 Choice of Layer Materials

The top layer material, $Al_{0.7}Ga_{0.3}As$, has an energy gap of 2.06 eV [28], a dielectric constant of 10.9 [28], and a lattice constant of 5.6588 Å [27]. So far, this material has been extensively used to fabricate heterojunction and tandem solar cells [20]. The reason behind choosing this material as the top layer material is its high bandgap. The top layer has been kept very thin (100 nm), and this layer plays a very minor role in optical absorption. Theoretically, it absorbs all the photons with energy greater than or equal to 2.06 eV, but it transmits all the photons having less energy than its bandgap [29]. Now, photons with energy less than 2.06 eV correspond to wavelength greater than 0.60 µm [30], which constitute a good portion of the solar spectrum. Besides this, the thinness of the top layer does not allow it to absorb a large number of photons, so a considerable number of photons with energy greater than 2.06 eV are supposed to surpass the top layer for being absorbed in the next layers.

The middle layer (absorber) material, $Al_{0.48}In_{0.52}As$, has a direct energy gap of 1.47 eV [26, 39], and a lattice constant of 5.8686 Å (lattice-matched to InP) [26]. This bandgap is near the optimum bandgap (1.4 eV) for a solar cell absorber [11]. 1.47 eV corresponds to a wavelength of 0.844 µm [30]. So, theoretically, the base layer will absorb all the photons with wavelength less than or equal to 0.844 µm. The highest wavelength present in visible light is around 0.78 µm, so it is evident that the middle layer absorbs the majority of photons transmitted from the top layer. To facilitate this absorption, the middle layer thickness is kept sufficiently high (10 µm), with respect to the top layer thickness. The issue of high lattice mismatch between $Al_{0.48}In_{0.52}As$ and $Al_{0.7}Ga_{0.3}As$ will be addressed in chapter 5.

A p-type$Ga_{0.67}In_{0.33}As$ layer was introduced later in the design, which, under high doping (1×10^{19} cm^{-3}), played the role of a Back Surface Field (BSF) layer. BSF layer is like a passivating layer for the rear surface of the cell. It has a much higher doping level than its adjacent layer, and their interface, as a result, acts like a barrier. An electric field is formed at the interface which prevents minority carrier flow from the base layer to the rear surface. So, the minority carrier concentration in the base is kept at higher levels [31].$Ga_{0.67}In_{0.33}As$ has a bandgap of 0.975 eV [28]. So, apart from providing passivation, this layer plays a less significant role in absorbing the photons with energy higher than 0.975 eV. As a total effect, after using this third layer, the output parameters are greatly improved. It is to be noted that the lattice constant of $Ga_{0.67}In_{0.33}As$ is 5.787 Å [27], which has 1.41% lattice mismatch with the upper $Al_{0.48}In_{0.52}As$ layer. This lattice mismatch issue will be taken care of in chapter 5.

2.2.2 **Choice of Substrate**

Germanium is a widely-used substrate for both heterojunction and multijunction solar cells. We needed to make a choice between Ge and GaAs as the substrate material. Germanium has almost the same lattice constant (5.658 Å) [28] as GaAs (5.65325 Å) [28]. The thermal expansion coefficients of these two materials are also similar. But the advantage that Germanium offers over GaAs as a substrate is its low cost and high mechanical strength. Due to this high mechanical strength, compared to GaAs, thinner Ge wafers can be fabricated [32].Now, there is significant lattice mismatch between Ge and $Ga_{0.67}In_{0.33}As$ (2.23%), which will be addressed in chapter 5.

2.2.3 **Results and Discussion for the Initial Design**

In the initial design, only two layers were used in the device. Thickness of the top $Al_{0.7}Ga_{0.3}As$ layer was 100 nm. It was heavily n-doped at a doping concentration of 1×10^{18} cm^{-3}. The bottom $Al_{0.48}In_{0.52}As$ layer (p-type) was 10 µm thick, and the doping concentration was kept at 1×10^{16} cm^{-3}. Germanium (Ge) substrate was used. Its p-type doping concentration was kept as 1×10^{16} cm^{-3}. Figure 2.1 below shows the light J-V characteristics graph obtained for this design.

Figure 2.1 shows that the initial design yields an open-circuit voltage (V_{oc}) of 0.5342 V, and the short-circuit current density (J_{sc}) is 15.63 mA/cm^2. Fill factor (FF) was calculated using the formula given in (6). For this simulation, the fill factor was calculated to be 0.8123.

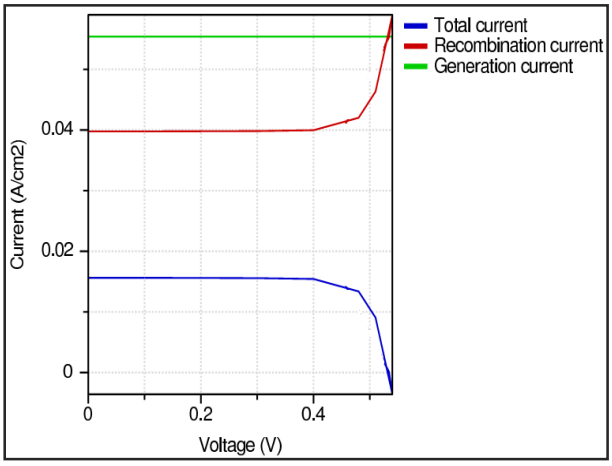

Fig. 2.1 Light J-V characteristics of the first design.

The working conditions for the solar cell (solar irradiance, temperature, concentration level) were considered as mentioned in section 1.1.3. The efficiency was calculated using equation (9). For this design, the calculated efficiency, $\eta = 6.78\%$.

Now, a third layer of p-type $Ga_{0.67}In_{0.33}As$ was introduced as the bottom layer. Layer thickness was taken as 3 μm, while the doping concentration was kept as 1×10^{16} cm^{-3}. At this doping level, the layer does not function as a passivation layer. It just facilitates additional absorption of photons, as discussed earlier. Parameters of all other layers were kept the same as the previous design. Figure 2.2 shows the light J-V characteristics graph obtained for this design.

It is seen from Figure 2.2 that, for the second design, both open-circuit voltage (V_{oc}) and short-circuit current density (J_{sc}) have increased to 0.8011 V and 22.19 mA/cm^2, respectively. The fill factor (FF) was 0.8606, and the efficiency (η) was calculated as 15.3%. Clearly, there is a large increase in the energy conversion efficiency due to the introduction of a third layer.

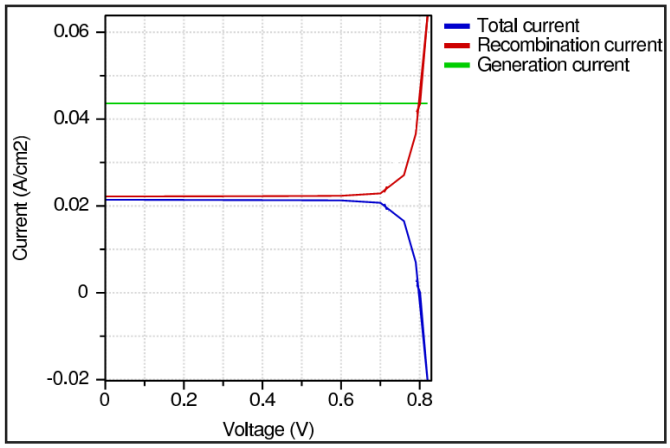

Fig. 2.2 Light J-V characteristics of the second design.

Now, a very high doping level (1×10^{19} cm^{-3}) was introduced in the $Ga_{0.67}In_{0.33}As$ bottom layer. This gives the dual effect of minimizing surface recombination and additional photon absorption in the bottom layer, as previously mentioned. Substrate doping level was changed to 1×10^{18} cm^{-3}. All other device parameters were kept the same as the previous design. For this design, the obtained light J-V characteristics graph is shown in Figure 2.3. From the figure, the values of open-circuit voltage and short-circuit current density are found to be 0.8959 V and 21.41 mA/cm^2, respectively. The fill factor in this case is 0.8719, and the calculated efficiency (η) is 16.79%. So, the efficiency is further improved due to the minimization of surface recombination at the rear surface.

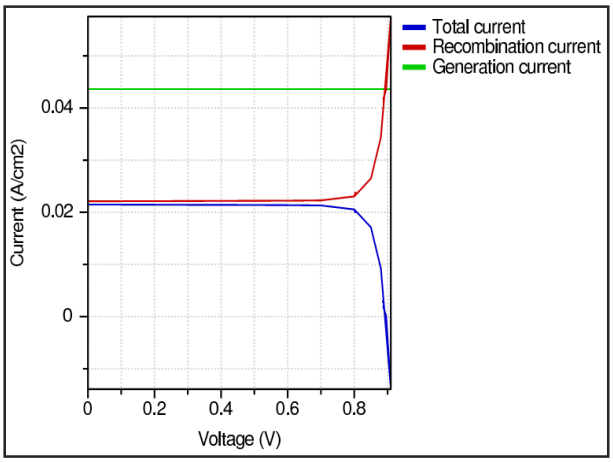

Fig. 2.3 Light J-V characteristics of the third design.

Figure 2.4 shows a schematic diagram of the heterojunction solar cell.

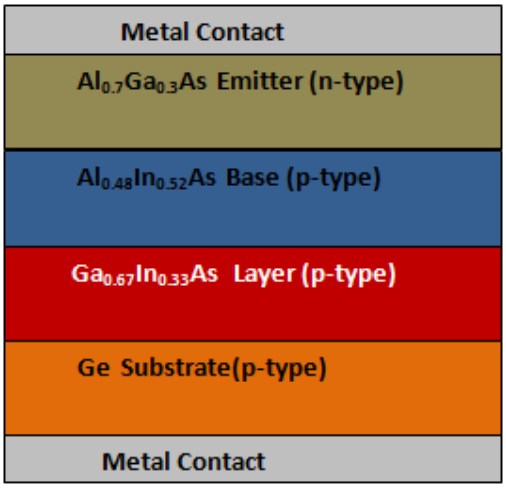

Fig. 2.4 Schematic diagram of the $Al_{0.7}Ga_{0.3}As/Al_{0.48}In_{0.52}As$ heterojunction solar cell.

Remarks

In this chapter, the light J-V characteristics curve of an initial design of the $Al_{0.7}Ga_{0.3}As/Al_{0.48}In_{0.52}As$ heterojunction solar cell has been simulated under AM1.5G illumination. The effect of introducing a $Ga_{0.67}In_{0.33}As$ BSF layer on the energy conversion efficiency has been illustrated through the simulation results. Finally, under 1 sun, an energy conversion efficiency of 16.79% has been reported, for the device shown schematically in Figure 2.4.

Chapter 3- Optimization of Device Parameters

3.3 Methodology

In this part of the work, device parameters (layer thickness and doping concentration) were optimized for each layer of the device. This was done by varying a particular parameter of a layer, while keeping every other device parameter fixed at some default value, and observing the changes in the output characteristics. Proper analysis of these changes led to the optimization of all the device parameters. Two optimized designs have been discussed at the end of this chapter.

At the beginning, some default values of layer thickness and doping level were chosen for each layer of the device shown in Figure 2.4. These default values are listed in table 3.1.

Simulation was conducted with these default values, and a light J-V characteristics graph was acquired. From the graph, values of open-circuit voltage (V_{oc}) and short-circuit current density (J_{sc}) were obtained. Fill factor (FF) and efficiency (η) were calculated using the equations (6) and (9), respectively. This efficiency is the efficiency under standard conditions, mentioned in section 1.1.3.

Table 3.1

Default Values of Device Parameters for the Heterojunction Solar Cell

Device Parameters	**Top Layer (Emitter) ($Al_{0.7}Ga_{0.3}As$)**	**Middle Layer (Base) ($Al_{0.48}In_{0.52}As$)**	**Bottom Layer ($Ga_{0.67}In_{0.33}As$)**	**Substrate (Ge)**
Layer Thickness (μm)	2	0.3	3	-
Doping Type	n	p	p	p
Doping Conc. (cm^{-3})	1×10^{18}	1×10^{16}	1×10^{16}	1×10^{18}

Now, the thickness of the bottom layer was varied, keeping all other device parameters fixed at their respective default values. For each different value of bottom layer thickness, a light J-V characteristics graph was obtained, and the efficiency was calculated using Equation (3). Then the efficiency was plotted against bottom layer thickness.

Afterwards, the thickness of the middle layer was varied, while every other device parameter was kept at its default value. Simulation was done for each different value of middle layer thickness. Efficiency was calculated for each simulation, and efficiency curve was obtained against varying middle layer thickness.

Now, thickness of the middle layer was varied, and for each different thickness, the top layer thickness was varied within a wide range. Efficiency was calculated for each combination of top and middle layer thickness values, and efficiency was plotted against top layer thickness. A number of curves were obtained, each for a particular middle layer thickness.

Now, simulations were done by changing the doping level in each layer, with all other values being kept as default, including the thickness. Finally, efficiency was plotted against varying doping level for each layer.

Analysing all the efficiency variation curves, two optimum designs have been proposed, which result in 19.57% and 20.56% efficiency, respectively.

3.4 Results and Discussions

3.4.1 Variation in Bottom Layer Thickness

Simulations were conducted for four different bottom layer thickness values: 0.2 μm, 1 μm, 2 μm and 3 μm (default value). Figures 3.1-3.4 show the respective light J-V characteristics curves for these simulations. From the graph in Figure 3.5, it was observed that the energy conversion efficiency is almost insensitive to the variation of bottom layer thickness, so further simulations were not conducted. Table 3.2 summarizes the simulation outcomes at varying values of bottom layer thickness.

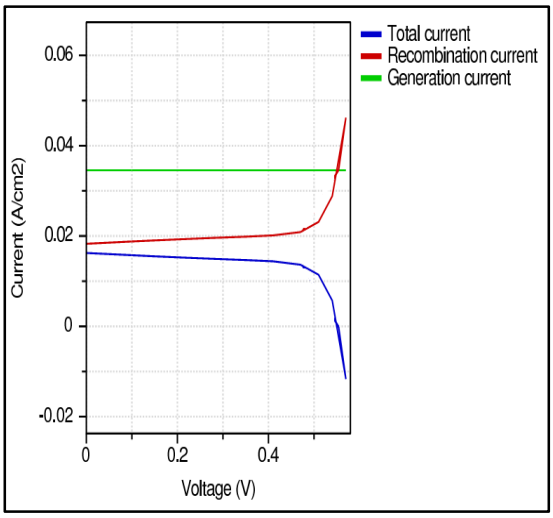

Fig. 3.1 Light J-V characteristics for bottom layer thickness = 0.2 µm.

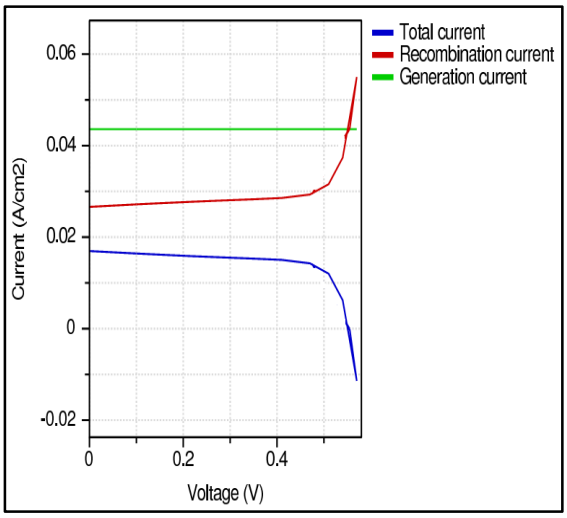

Fig. 3.3 Light J-V characteristics for bottom layer thickness = 2µm.

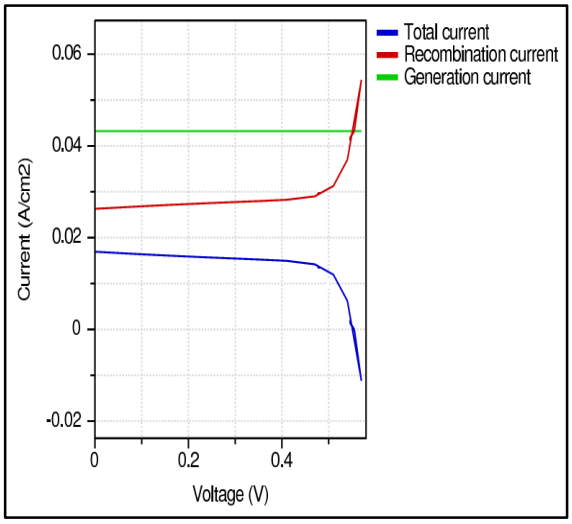

Fig. 3.2 Light J-V characteristics for bottom layer thickness = 1µm.

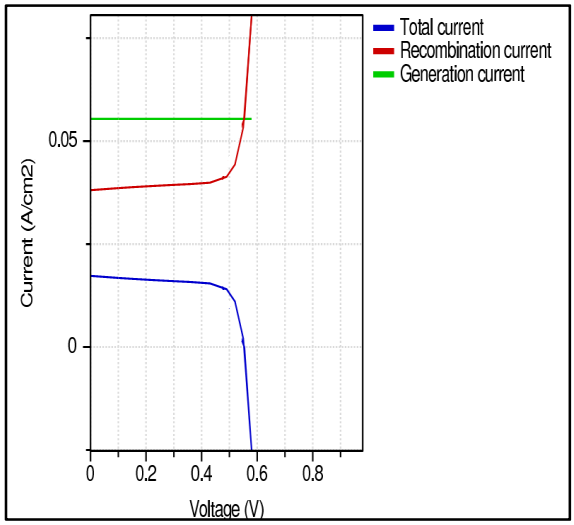

Fig. 3.4 Light J-V characteristics for bottom layer thickness = 3 µm.

Table 3.2

Simulation Outcomes for varying Bottom Layer Thickness

Bottom Layer Thickness (µm)	**V_{oc} (V)**	**J_{sc} (mA/cm^2)**	**FF**	**Efficiency (η%)**
0.2	0.555	16.9	0.8174	7.67
1	0.55	17.2	0.8162	7.72
2	0.551	17.1	0.8165	7.69
3	0.5539	17.29	0.8172	7.83

The efficiency versus bottom layer thickness graph is given in Figure 3.5. It is evident that efficiency is almost insensitive to variation in bottom layer thickness. This is because of the fact that the bottom layer mainly serves as a Back Surface Field (BSF) layer [31] when it has a much higher doping with respect to the middle layer. But its role in optical absorption is insignificant, compared to the middle (Base) layer. So, thickness variation at the bottom layer does not have any significant impact on cell efficiency.

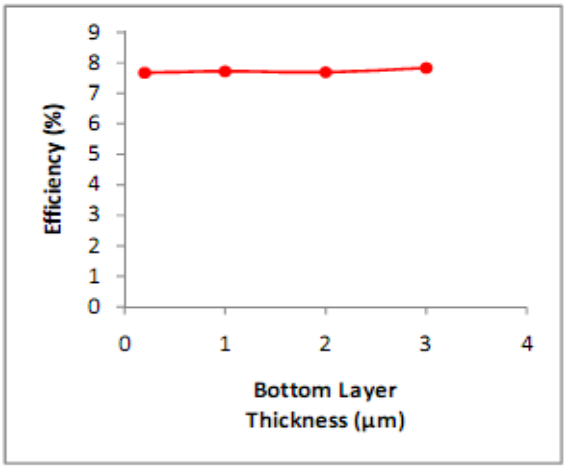

Fig. 3.5 Graph of efficiency vs bottom layer thickness.

3.4.2 Variation in Middle Layer Thickness

Middle layer thickness was varied within the wide range of 0.3 µm to 20 µm. Simulation outcomes for varying middle layer thickness are summarized in table 3.3.

Table 3.3

Simulation Results for Varying Middle Layer Thickness

Middle Layer Thickness (µm)	**V_{oc} (V)**	**J_{sc} (mA/cm^2)**	**FF**	**Efficiency (η%)**
0.3	0.5539	17.29	0.8172	7.83
2	0.7506	13.93	0.8536	8.93
3	0.7651	14.71	0.8557	9.62
10	0.8014	15.67	0.8606	10.82
20	0.8214	15.83	0.8632	11.22

Figures 3.6-3.10 show the respective light J-V characteristics curves for all the simulations of table 3.3.

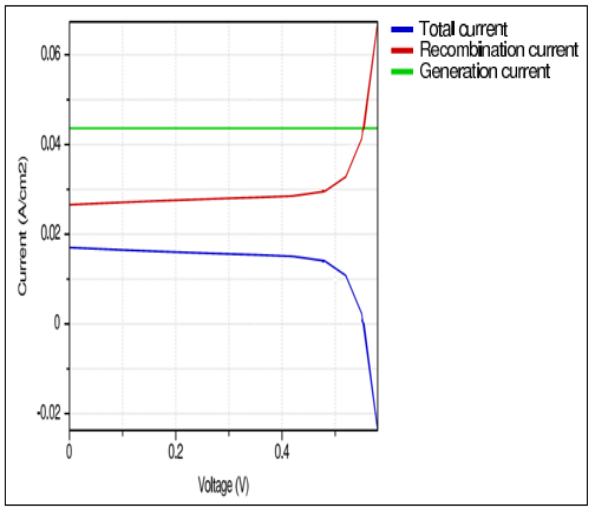

Fig. 3.6 Light J-V characteristics for middle layer thickness = 0.3 µm.

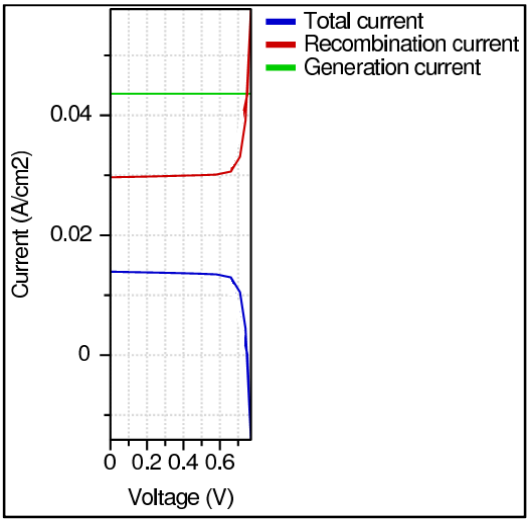

Fig. 3.7 Light J-V characteristics for middle layer thickness = 2 µm.

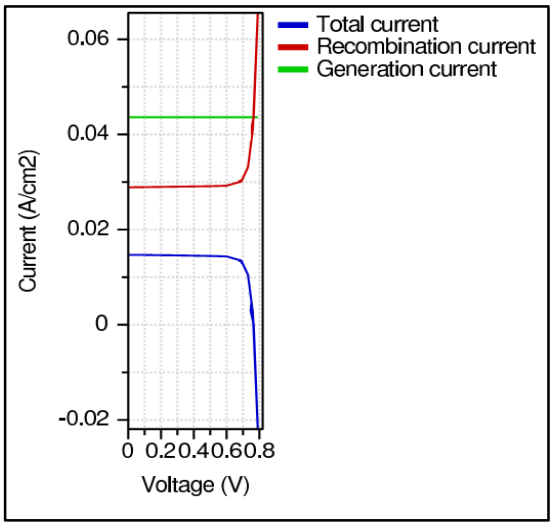

Fig. 3.8 Light J-V characteristics for middle layer thickness = 3 µm.

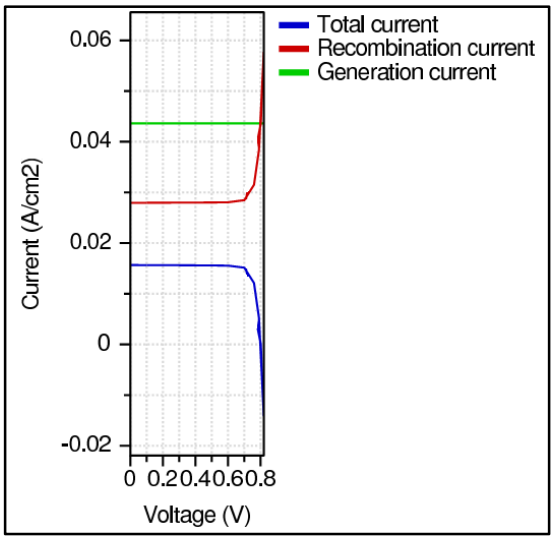

Fig. 3.9 Light J-V characteristics for middle layer thickness = 10 µm.

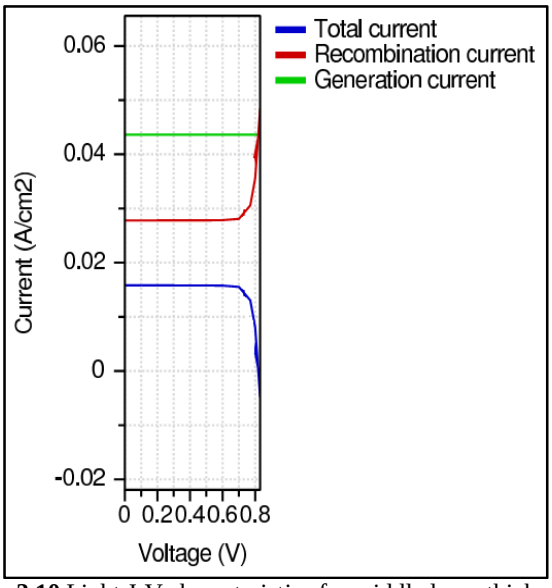

Fig. 3.10 Light J-V characteristics for middle layer thickness = 20 µm.

The efficiency versus middle layer thickness graph is given in Figure 3.11.

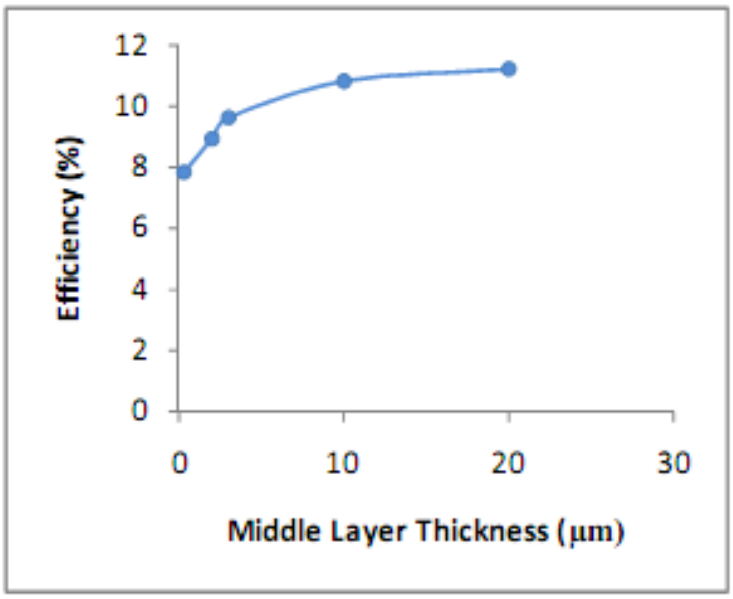

Fig. 3.11 Graph of efficiency vs middle layer thickness.

As it is seen from Figure 3.11, efficiency increases with increasing middle layer thickness. Actually, this is an already established fact [33], because a greater number of photons can be absorbed by a thicker base. The target here was to analyse the degree of variation in efficiency, and move towards an optimization of the base layer thickness for high efficiency.

3.4.3 Variation in Top Layer Thickness (with Fixed Middle Layer Thickness)

Now, the top layer thickness was varied within a range for a certain base layer thickness. Then, the base (middle) layer thickness was changed to another fixed value, and, for this, the top layer thickness was varied again within the same range. This process was conducted for a total of three base layer thickness values. Tables 3.4, 3.5 and 3.6 summarize the simulation outcomes. The light J-V characteristics curves for all these simulations are given in figures 3.12- 3.26.

Table 3.4

Simulation Outcomes for Varying Top Layer Thickness (Middle Layer Thickness = 5 Micron)

Top Layer Thickness (µm)	**V_{oc} (V)**	**J_{sc} (mA/cm^2)**	**FF**	**Efficiency (η%)**
1	0.7812	15.62	0.8579	10.48
0.5	0.7812	16.71	0.8579	11.2
0.1	0.7809	21.03	0.8579	14.09
0.05	0.7809	22.46	0.8579	15.04
0.01	0.7806	23.88	0.8579	15.99

Table 3.5

Simulation Results for varying Top Layer Thickness (Middle Layer Thickness = 10 Micron)

Top Layer Thickness (µm)	**V_{oc} (V)**	**J_{sc} (mA/cm^2)**	**FF**	**Efficiency (η%)**
1	0.8015	15.99	0.8606	11.03
0.5	0.8015	17.08	0.8606	11.78
0.1	0.8011	22.19	0.8606	15.3
0.05	0.8009	22.86	0.8606	15.76
0.01	0.8006	24.29	0.8605	16.73

Table 3.6

Simulation Outcomes for varying Top Layer Thickness (Middle Layer Thickness = 20 Micron)

Top Layer Thickness (µm)	**V_{oc} (V)**	**J_{sc} (mA/cm^2)**	**FF**	**Efficiency (η%)**
1	0.8214	16.15	0.8632	11.46
0.5	0.8213	17.23	0.8632	12.21
0.1	0.8208	22.02	0.8631	15.64
0.05	0.8206	23.03	0.8631	16.3
0.01	0.8203	24.47	0.863	17.32

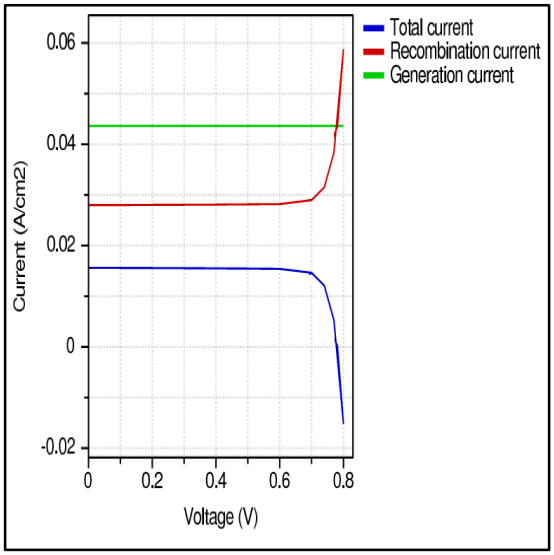

Fig. 3.12 Light J-V characteristics for top layer thickness = 1 µm (with middle layer thickness = 5 µm).

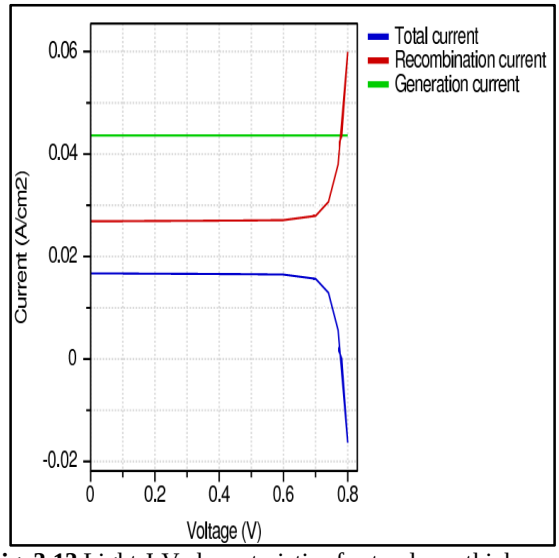

Fig. 3.13 Light J-V characteristics for top layer thickness = 0.5 µm (with middle layer thickness = 5 µm).

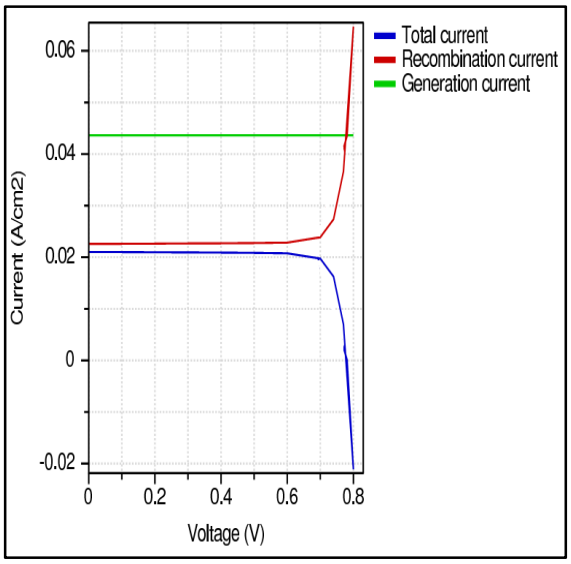

Fig. 3.14 Light J-V characteristics for top layer thickness = 0.1 µm (with middle layer thickness = 5 µm).

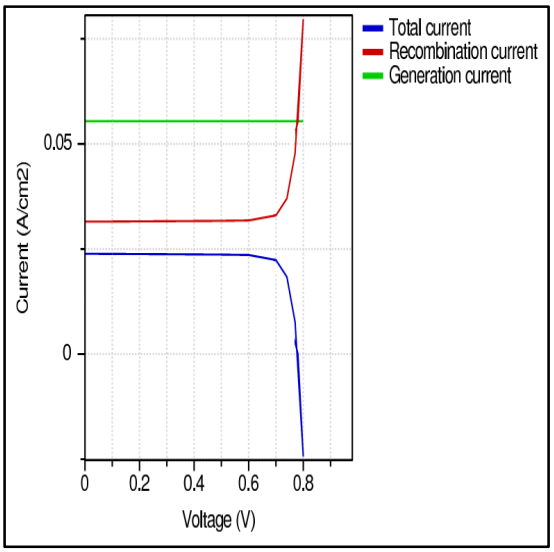

Fig. 3.16 Light J-V characteristics for top layer thickness = 0.01 µm (with middle layer thickness = 5 µm).

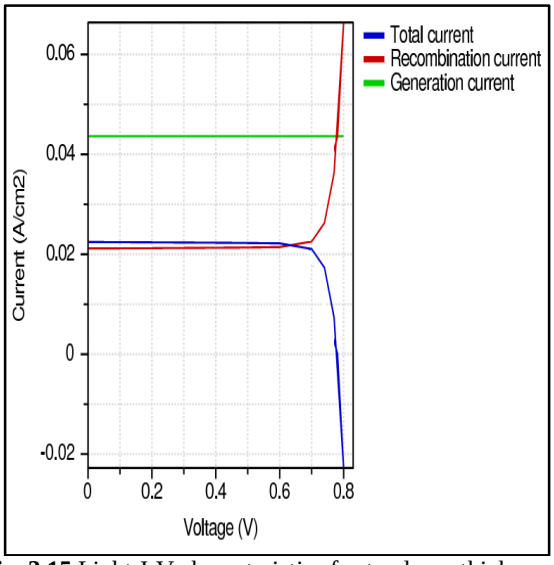

Fig. 3.15 Light J-V characteristics for top layer thickness = 0.05 µm (with middle layer thickness = 5 µm).

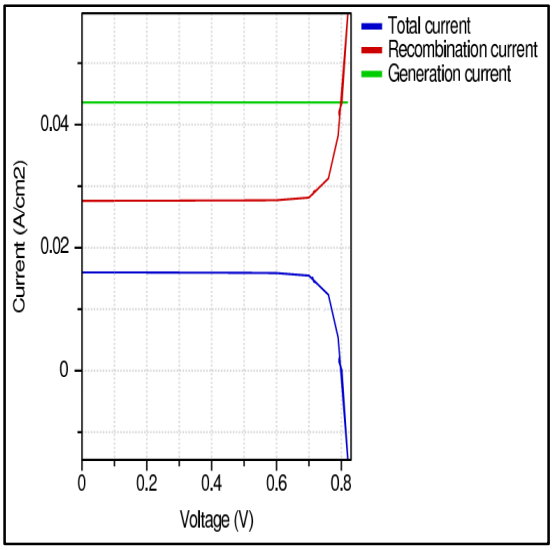

Fig. 3.17 Light J-V characteristics for top layer thickness = 1 µm (with middle layer thickness = 10 µm).

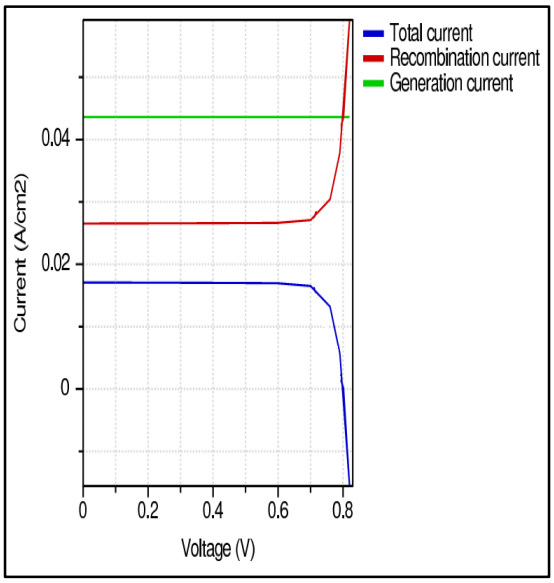

Fig. 3.18 Light J-V characteristics for top layer thickness = 0.5 µm (with middle layer thickness = 10 µm).

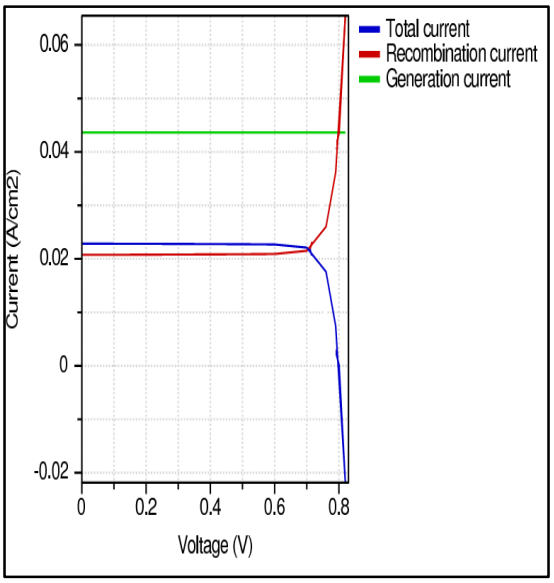

Fig. 3.20 Light J-V characteristics for top layer thickness = 0.05 µm (with middle layer thickness = 10 µm).

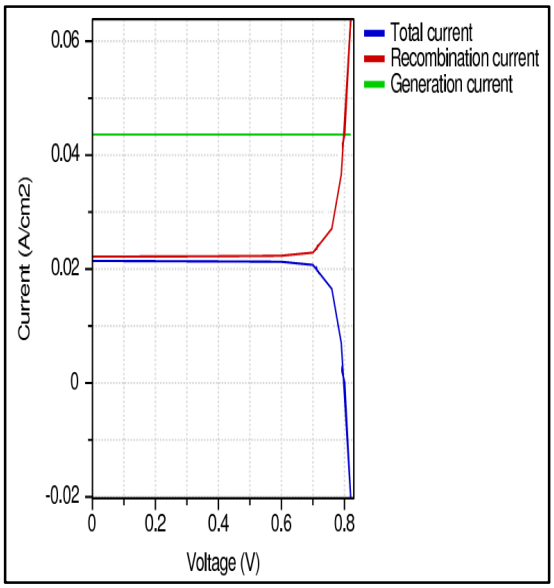

Fig. 3.19 Light J-V characteristics for top layer thickness = 0.1 µm (with middle layer thickness = 10 µm).

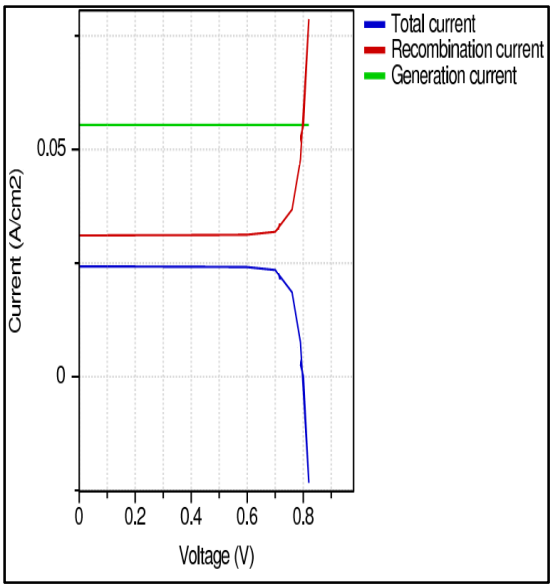

Fig. 3.21 Light J-V characteristics for top layer thickness = 0.01 µm (with middle layer thickness = 10 µm).

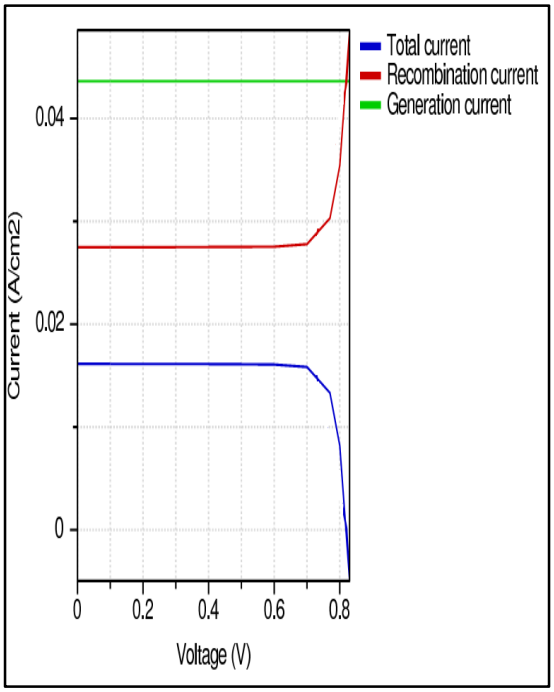

Fig. 3.22 Light J-V characteristics for top layer thickness = 1 µm (with middle layer thickness = 20 µm).

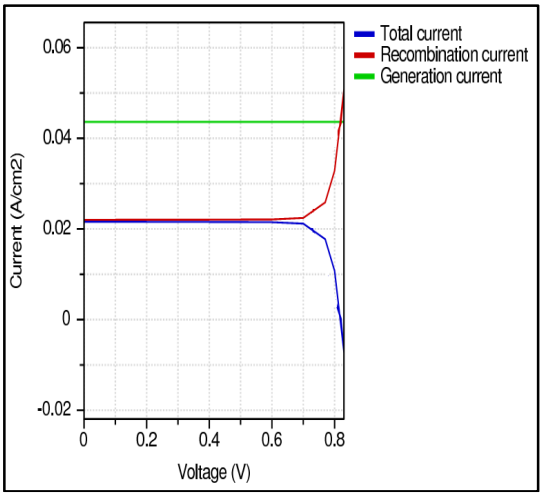

Fig. 3.24 Light J-V characteristics for top layer thickness = 0.1 µm (with middle layer thickness = 20 µm).

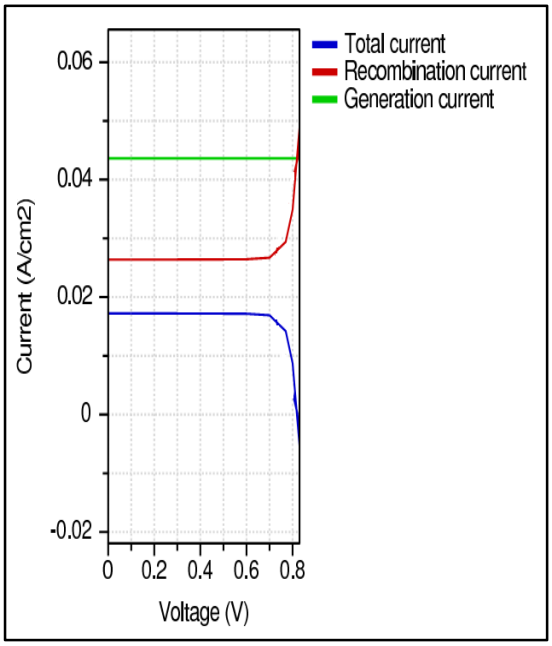

Fig. 3.23 Light J-V characteristics for top layer thickness = 0.5 µm (with middle layer thickness = 20 µm).

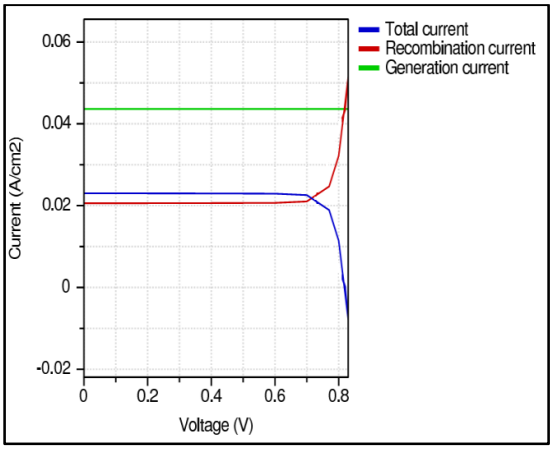

Fig. 3.25 Light J-V characteristics for top layer thickness = 0.05 µm (with middle layer thickness = 20 µm).

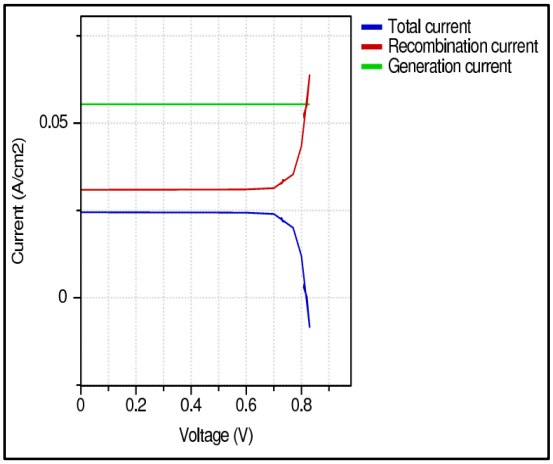

Fig. 3.26 Light J-V characteristics for top layer thickness = 0.01 µm (with middle layer thickness = 20 µm).

Figure 3.27 shows the efficiency versus top layer thickness curves (base layer thickness value is fixed for each curve). As it is seen from the figure, efficiency decreases with increasing top layer thickness. This is an expected outcome, because the top layer actually acts like a window layer [29]. Short-circuit current and optical absorption capability of the device is improved with a thinner window layer [34], which is supported by table 3.6. So, minimization of top layer thickness, and maximization of base layer thickness will be an important step towards optimization.

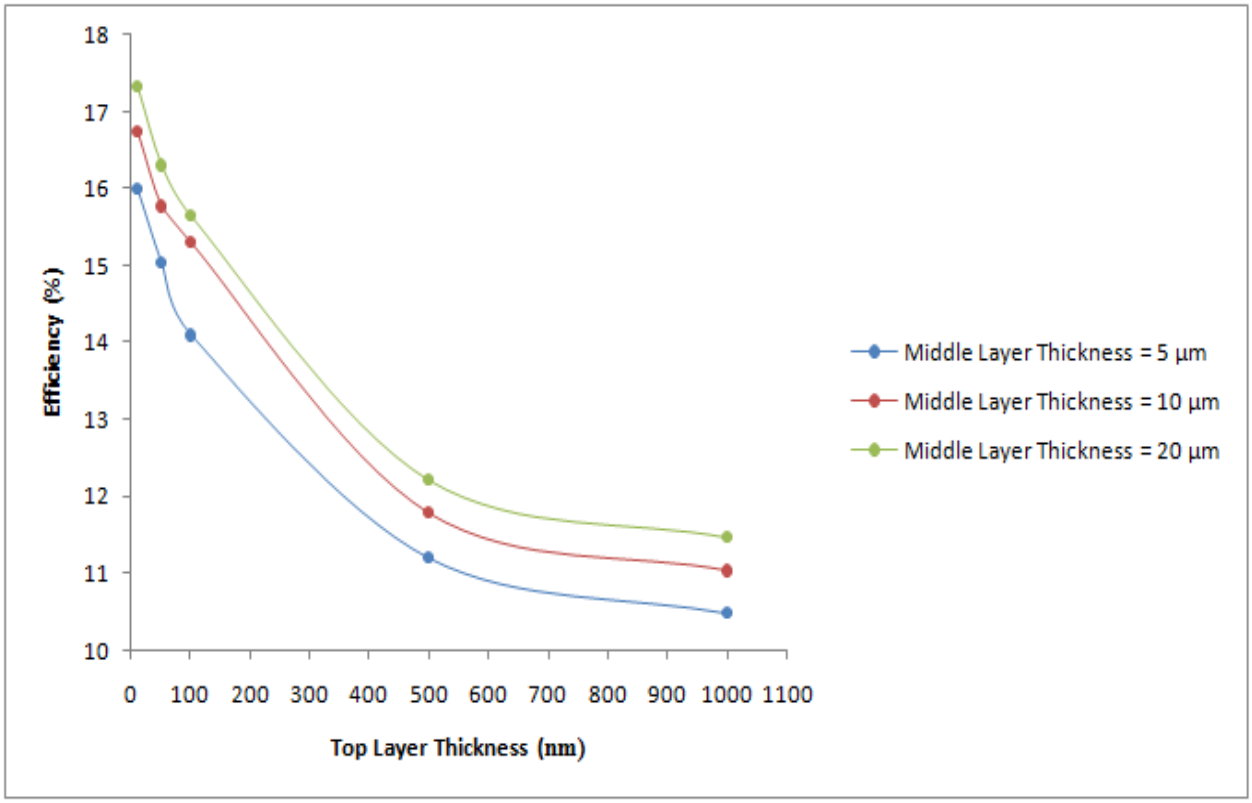

Fig. 3.27 Graph of efficiency vs top layer thickness.

3.4.4 Variation in Top Layer Doping Concentration

The doping level of the n-type emitter layer was varied within a range of $1\times10^{16}cm^{-3}$ to $1\times10^{19}\,cm^{-3}$, and efficiency was calculated for each different value. It is to be noted that all other device parameters, including the layer thickness values, were kept as default. Table 3.7 summarizes the simulation outcomes. The light J-V characteristics curves for these simulations are given in figures 3.28- 3.31.

Table 3.7

Simulation Results for Varying Doping Levels at the Top Layer

n-type Doping Conc. (cm^{-3})	**V_{oc} (V)**	**J_{sc} (mA/ cm^2)**	**FF**	**Efficiency (η%)**
1×10^{16}	0.562	14.6	0.8191	6.72
1×10^{17}	0.5562	16.34	0.8177	7.43
1×10^{18}	0.5539	17.29	0.8172	7.83
1×10^{19}	0.5537	17.36	0.8171	7.86

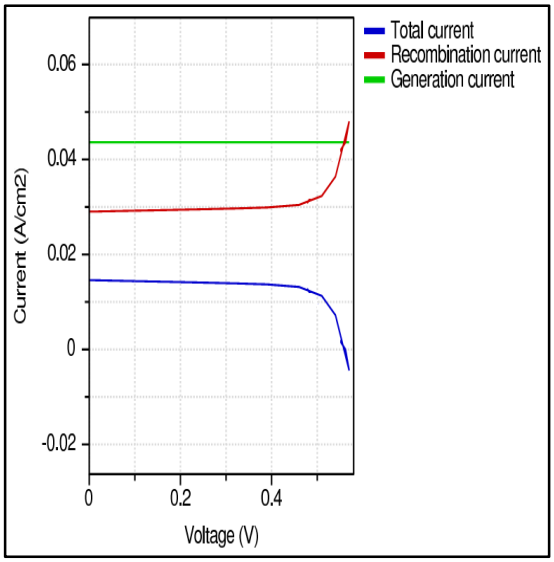

Fig. 3.28 Light J-V characteristics for top layer doping concentration = 1×10^{16} cm^{-3}.

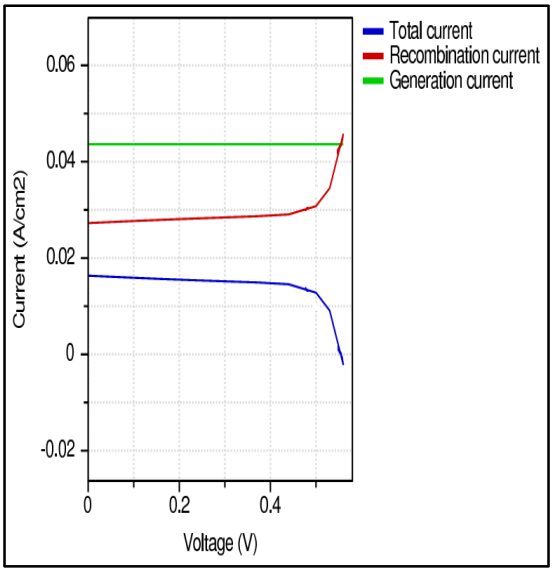

Fig. 3.29 Light J-V characteristics for top layer doping concentration = 1×10^{17} cm^{-3}.

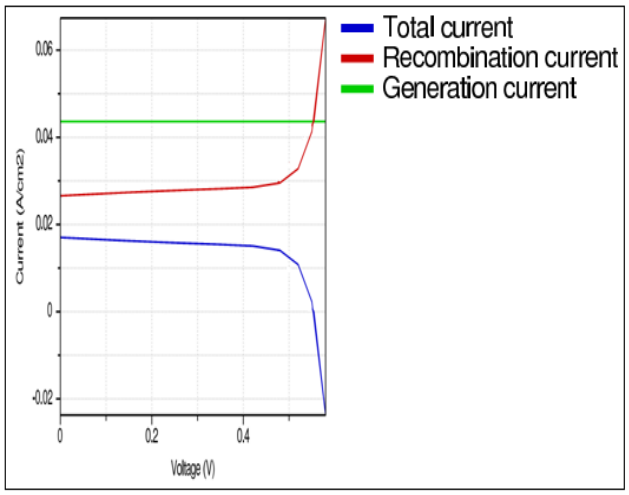

Fig. 3.30 Light J-V characteristics for top layer doping concentration = 1×10^{18} cm^{-3}.

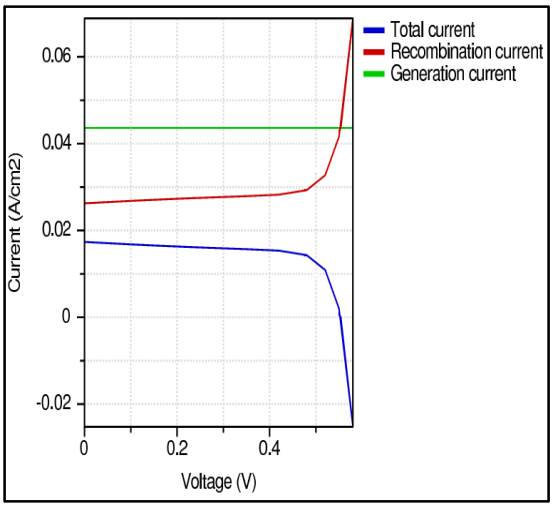

Fig. 3.31 Light J-V characteristics for top layer doping concentration = 1×10^{19} cm^{-3}.

Figure 3.32 shows a plot of efficiency versus top layer doping level. From the figure, it is evident that efficiency increases with increasing doping level in the top layer. The fact of efficiency increment with high doping level in the window layer has been supported by previous works [35] [36]. The $Al_xGa_{1-x}As$ emitter forms an n-p junction with the $Al_xIn_{1-x}As$ base, and an increased doping in the emitter increases the electric field in the space-charge region, which, in turn, increases the drift velocity of the majority carriers. This increased drift velocity increases the output current. But at the same time, a higher doping level at the emitter increases the minority carrier recombination rate [36], which reduces the output current. So, the change in output current depends on which of these two factors dominates the other at a particular doping concentration. As it is seen from table 3.7, short-circuit current keeps on increasing significantly, as the doping increases in the emitter. This implies that at increased doping, the increased electric field has a much stronger effect than the minority carrier recombination. So, for optimization, the top layer doping level should be kept as high as possible.

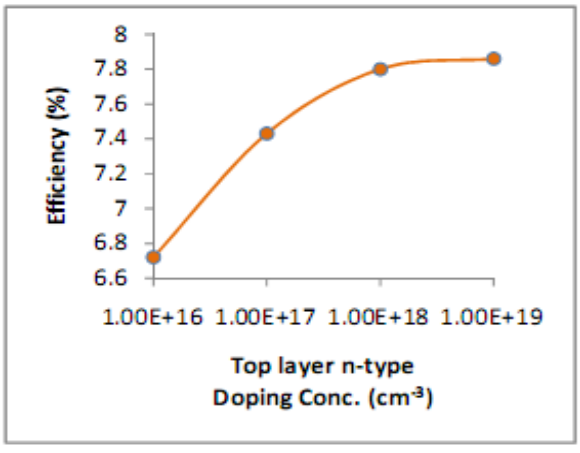

Fig. 3.32 Graph of efficiency versus top layer doping level.

3.4.5 Variation in Middle Layer Doping Concentration

Now, the doping concentration in the base layer was varied (from 1×10^{16}cm^{-3} to 1×10^{18} cm^{-3}), keeping every other device parameter as default. The results are shown in table 3.8. Light J-V characteristics curves for all these simulations are shown in figures 3.33- 3.35.

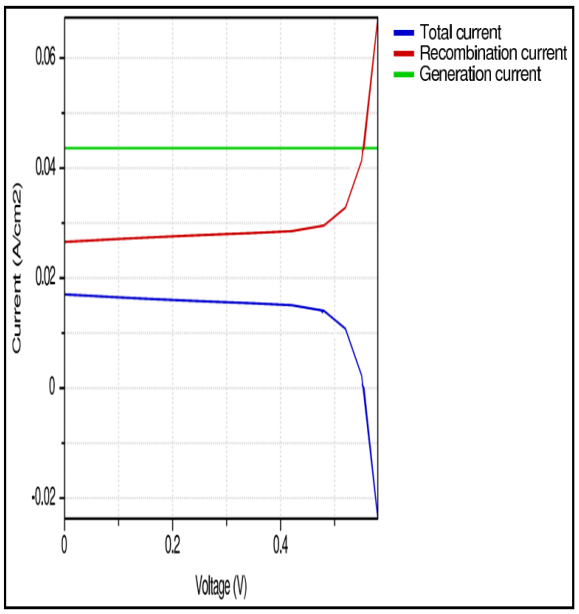

Fig. 3.33 Light J-V characteristics for middle layer doping concentration = 1×10^{16} cm^{-3}.

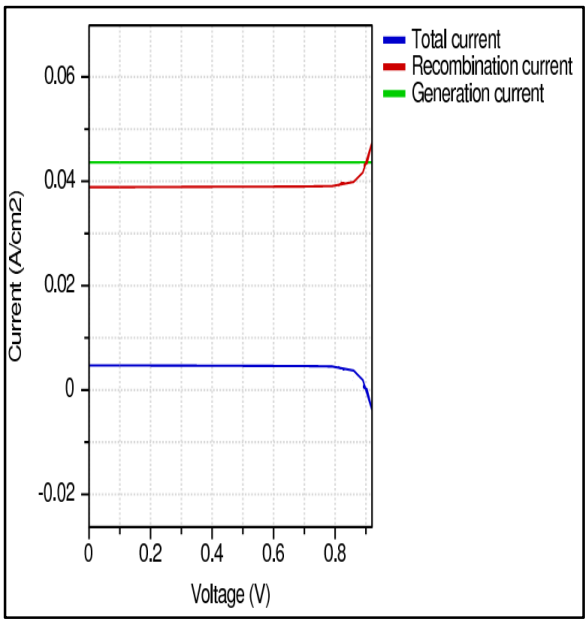

Fig. 3.35 Light J-V characteristics for middle layer doping concentration = 1×10^{18} cm^{-3}.

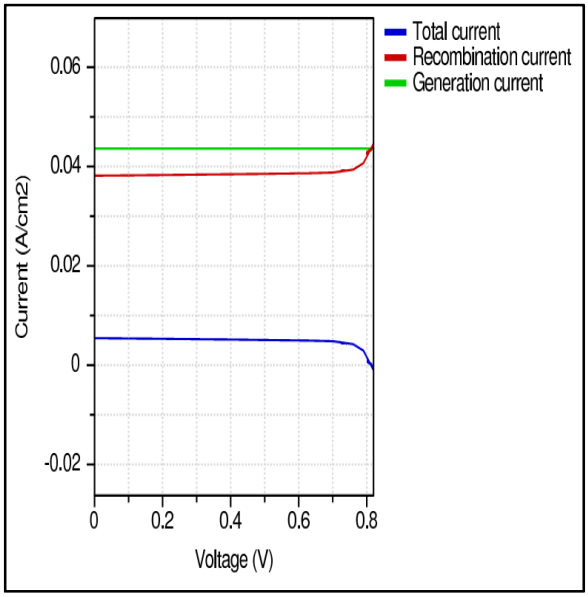

Fig. 3.34 Light J-V characteristics for middle layer doping concentration = 1×10^{17} cm^{-3}.

Table 3.8

Simulation Results for Doping Conc. Variation at the Middle Layer

p-type Doping Conc. (cm^{-3})	**V_{oc} (V)**	**J_{sc} (mA/ cm^2)**	**FF**	**Efficiency (η%)**
1×10^{16}	0.5539	17.29	0.8172	7.83
1×10^{17}	0.8149	5.443	0.8624	3.82
1×10^{18}	0.9041	4.736	0.8727	3.74

A graph of efficiency versus middle layer doping level is given in Figure 3.36. It is evident from the figure that the efficiency decreases with increasing doping concentration in the base layer. Actually, the base is pretty thick, and an increased minority carrier recombination rate in the base due to high doping has a strong negative impact on the output current. This negative impact cannot be compensated by the increased electric field at high doping. As a result, the output current decreases with increased base doping, which is supported by table 3.8. The same type of effect was observed in a previous work with GaAs solar cells [37], which forced a low-level doping in the base for optimization. As the intrinsic carrier concentration of $Al_{0.48}In_{0.52}As$ is pretty high, we restrict the optimized doping level in the base to $1\times10^{16}cm^{-3}$.

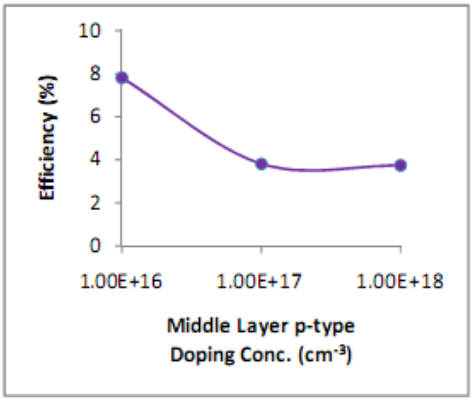

Fig. 3.36 Graph of efficiency versus middle layer doping level.

3.4.6 Variation in Bottom Layer Doping Concentration

To understand the effect of variation in bottom layer doping level on efficiency, simulations were conducted with varying bottom layer doping concentrations (from 1×10^{16}cm^{-3} to 1×10^{19} cm^{-3}). The outcomes are summarized in table 3.9. Light J-V characteristics curves for these simulations are shown in figures 3.37- 3.40.

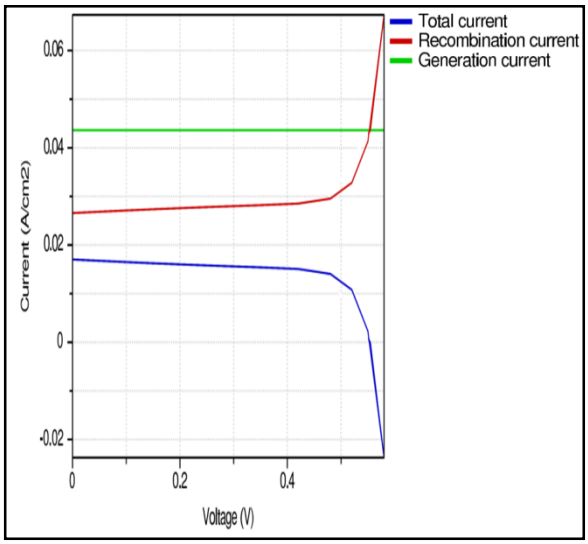

Fig. 3.37 Light J-V characteristics for bottom layer doping concentration = 1×10^{16} cm^{-3}.

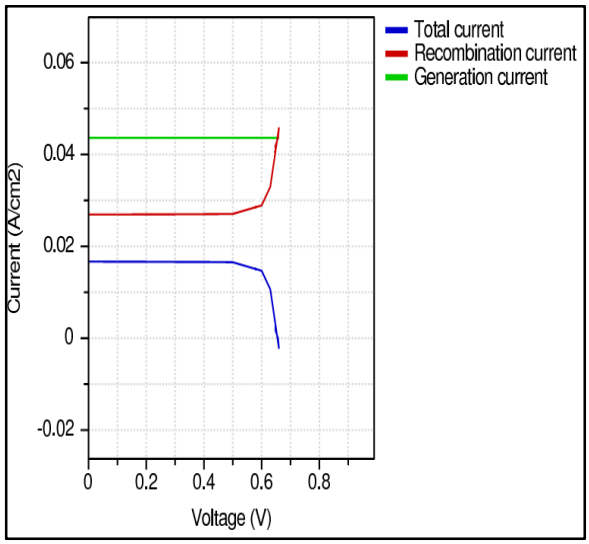

Fig. 3.39 Light J-V characteristics for bottom layer doping concentration = 1×10^{18} cm^{-3}.

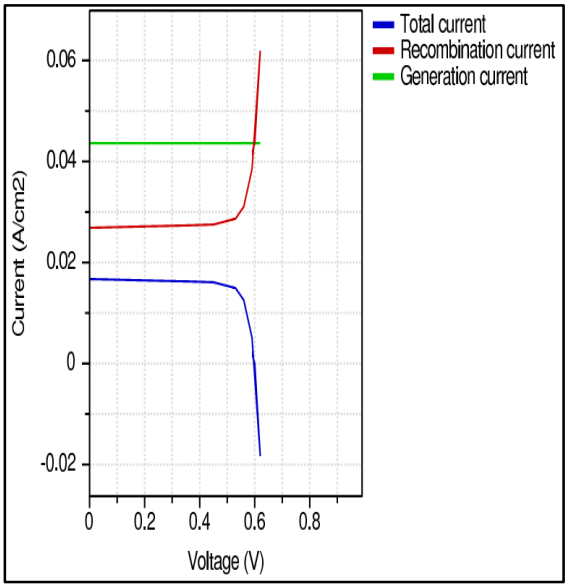

Fig. 3.38 Light J-V characteristics for bottom layer doping concentration = 1×10^{17} cm^{-3}.

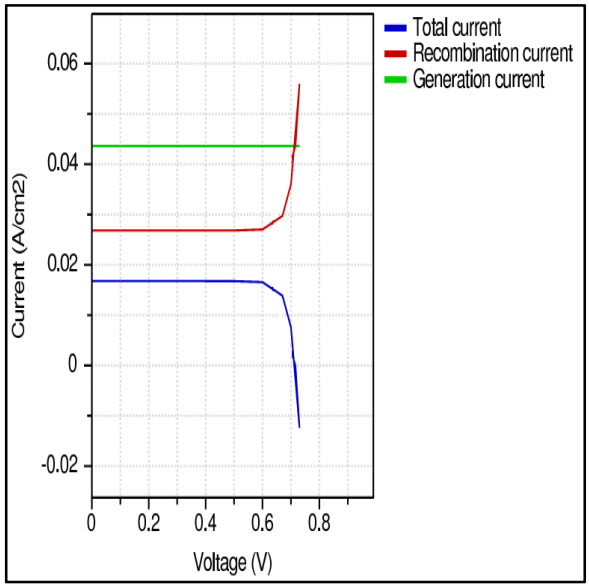

Fig. 3.40 Light J-V characteristics for bottom layer doping concentration = 1×10^{19} cm^{-3}.

Figure 3.41 shows a plot of efficiency versus bottom layer doping level. The graph shows that efficiency is increased at high doping levels in the bottom layer. This happens because, under high doping, the bottom layer acts as a Back Surface Field (BSF) layer. The BSF layer is a passivating layer that restricts the flow of minority carriers from the base to the rear surface of the cell [31]. As a result, surface recombination of these minority carriers is minimized, and the short-circuit current density (J_{sc}) is increased. So, the efficiency is increased as well. For optimization towards higher efficiency, the doping level at the bottom layer should be kept as high as possible.

Table 3.9

Simulation Results for Varying Doping Levels at the Bottom Layer

p-type Doping Conc. (cm^{-3})	**V_{oc} (V)**	**J_{sc} (mA/ cm^2)**	**FF**	**Efficiency (η%)**
1×10^{16}	0.5539	17.29	0.8172	7.83
1×10^{17}	0.6	16.73	0.8274	8.31
1×10^{18}	0.6566	16.68	0.8384	9.18
1×10^{19}	0.7156	16.79	0.8484	10.19

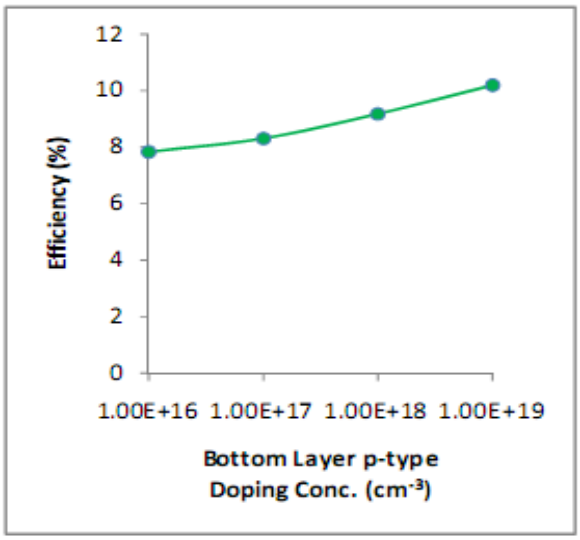

Fig. 3.41 Graph of efficiency versus bottom layer doping level.

3.4.7 Design Optimization

Using the analysis of the efficiency variation curves, two optimum designs have been proposed. The first design yields an energy conversion efficiency of 20.56%, while the second design gives 19.57% efficiency. The advantage of the second design over the first one is its lower fabrication cost, due to the requirement of less material.

3.4.7.1 First Design

After analysing all the types of efficiency variation curves obtained, an optimum design has been proposed, which uses a very thin emitter ($Al_{0.7}Ga_{0.3}As$) layer of 10 nm thickness. The base ($Al_{0.48}In_{0.52}As$) layer is made very thick (100 µm) for maximum optical absorption. The bottom layer ($Ga_{0.67}In_{0.33}As$) has a thickness of 3 µm. Doping concentration is kept very high at the top and bottom layers (1×10^{19} cm^{-3} for both layers), while the base is doped lightly (1×10^{16} cm^{-3}). Figure 3.42 shows the light J-V characteristics graph obtained for this design.

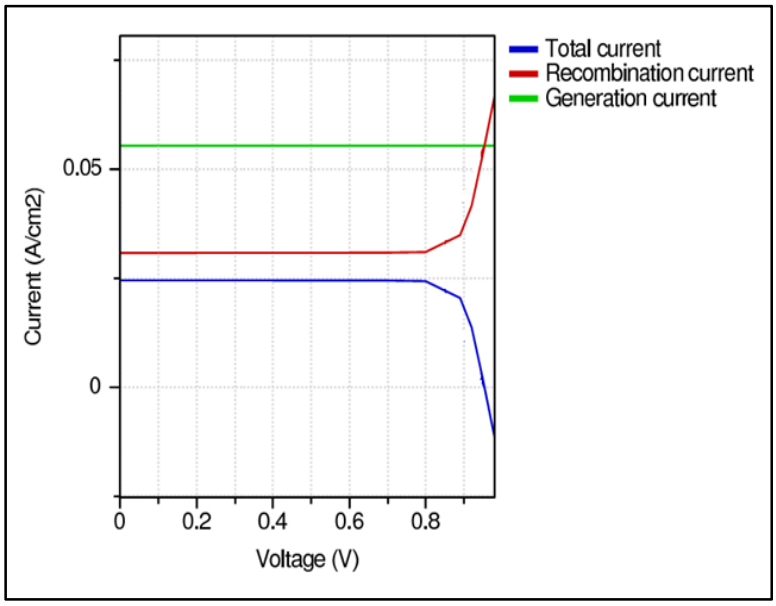

Fig. 3.42 Light J-V characteristics for the first optimized design.

From Figure 3.42, it is found that the resulting open-circiut voltage (V_{oc}) is 0.9535 V, and the short-circuit current density (J_{sc}) is 24.56 mA/cm^2. The fill factor (FF) is calculated to be 0.8606, and the calculated efficiency (η) is 20.56%.

3.4.7.2 Second Design

In the second design, all the design parameters are kept the same as the first design, except the base layer thickness, which is reduced to 20 µm. Figure 3.43 shows the light J-V characteristics curve obtained for this design.

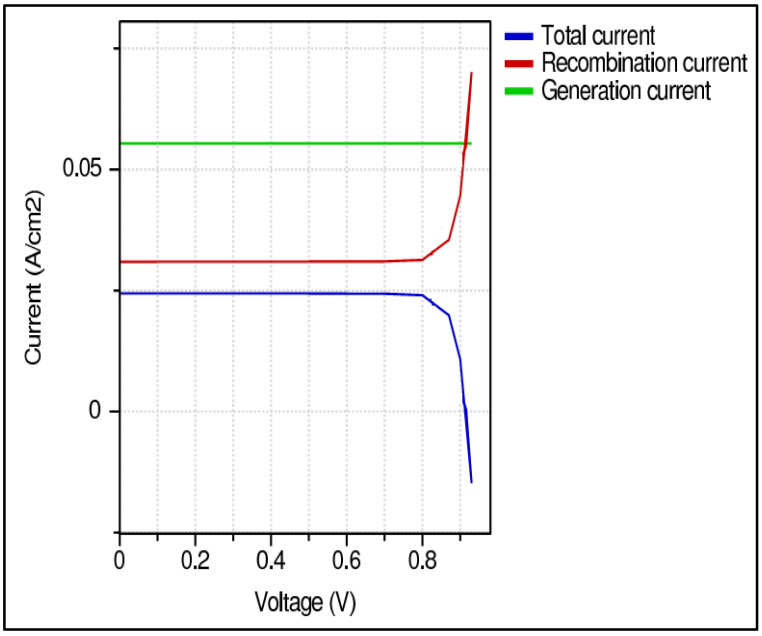

Fig. 3.43 Light J-V characteristics for the second optimized design.

For this design, an open-circuit voltage (V_{oc}) of 0.9162 has been obtained, while the short-circuit current density (J_{sc}) is 24.44 mA/cm^2. The fill factor is 0.874, and the efficiency is calculated to be 19.57%.

In the heterojunction solar cell, every other layer is much thinner than the base layer. So, an 80 µm thickness reduction in the base will greatly reduce the fabrication cost, and it can be a good trade-off with the small loss in efficiency (19.57% from 20.56%).

Remarks

This chapter presents an extensive analysis with relevant data and figures of the dependence of efficiency on layer thickness and doping concentration of each layer of the device. The information provided here will be helpful later in the fabrication of photovoltaic cells using an $Al_{0.7}Ga_{0.3}As/Al_{0.48}In_{0.52}As$ heterojunction, or any other heterojunction of III-V ternary alloys. These will also provide a better understanding of design optimization in heterojunction solar cells.

Chapter 4- Optimization of Alloy Composition

4.4 Insight

The electrical properties of III-V ternary alloys such as bandgap, carrier mobility, dielectric constant [28] etc. can be greatly varied by changing the alloy composition. This change also affects various optical properties like absorption coefficient [28], refractive index [27] etc. In this chapter, simulation results have been analysed for varying alloy compositions of the three ternary alloys- $Al_xGa_{1-x}As$, $Al_xIn_{1-x}As$ and $Ga_xIn_{1-x}As$, which constitute the solar cell. The top layer material, $Al_xGa_{1-x}As$, can have a varying energy gap of 1.55-2.13 eV, as the Aluminium mole fraction x varies from 0.1 to 0.9. It becomes a direct bandgap material from an indirect one as x becomes lower, the transition point located at x= 0.45 [28]. Energy gap of the base layer material, $Al_xIn_{1-x}As$, varies from 0.5 to 2.05 eV, as x varies between 0.1 and 0.9 [38]. As x becomes higher, this material changes from direct to indirect, the transition point being located at $x \approx 0.63$ [38]. For $Ga_xIn_{1-x}As$, an energy gap variation between 0.43-1.28 eV is possible for variation of x (Gallium mole fraction) between 0.1-0.9 [39]. $Ga_xIn_{1-x}As$ is a direct material, for all values of x [28]. Besides bandgap, change in alloy composition alters many other electrical and optical properties of an alloy, as previously mentioned. Hence, an analysis of efficiency variation of the device with changing alloy composition at the layers can give an insight on how the alloy composition should be fixed at each layer for the maximization of energy conversion efficiency.

4.5 Methodology

Before conducting simulations, some default values for thickness, doping concentration and alloy composition for each layer were fixed. Table 4.1 summarizes these default values.

Now, simulations were conducted by varying the value of x for the top layer alloy ($Al_xGa_{1-x}As$) from 0.1 to 0.9, in steps of 0.1. For each simulation, value of every other device parameter was kept the same as listed in table 4.1. Now, a light J-V characteristics curve was obtained for every simulation, which was used to calculate the energy conversion efficiency for that particular simulation. In this manner, efficiency for each of the simulations was obtained. Then, efficiency was plotted against x (Aluminium mole fraction) for the top layer. The efficiency curve was analysed for getting an idea about the optimization of Aluminium mole fraction in $Al_xGa_{1-x}As$ for achieving higher efficiency.

Table 4.1

Default Values of Device Parameters for Each Layer

Device Parameters	**Top Layer (Emitter) ($Al_xGa_{1-x}As$)**	**Middle Layer (Base) ($Al_xIn_{1-x}As$)**	**Bottom Layer (BSF Layer) ($Ga_xIn_{1-x}As$)**	**Substrate (Ge)**
Layer Thickness (μm)	0.01	100	3	-
Doping Type	n	p	p	p
Doping Conc. (cm^{-3})	1×10^{19}	1×10^{16}	1×10^{19}	1×10^{18}
Value of x for the Alloy	0.7	0.48	0.67	-

Afterwards, simulations were done by varying the value of x for the base layer alloy ($Al_xIn_{1-x}As$) from 0.1 to 0.6, in steps of 0.1. Efficiency versus x (Aluminium mole fraction) curve was obtained in the similar manner discussed above. Further simulations (for x=0.7 to 0.9) were not conducted, as the nature of efficiency variation against varying alloy composition was already evident from the graph.

Afterwards, x (Gallium mole fraction) was varied for $Ga_xIn_{1-x}As$ in the bottom layer, from 0.1 to 0.9, in steps of 0.1. The efficiency curve obtained in this case gave an insight about the optimization of Gallium mole fraction in $Ga_xIn_{1-x}As$. Finally, after combining all these outcomes, three optimized designs have been proposed, the best one yielding 21.39% efficiency.

4.6 Results and Discussions

4.6.1 Varying Alloy Composition in $Al_xGa_{1-x}As$ (Top Layer)

Aluminium mole fraction x, in $Al_xGa_{1-x}As$, was varied from 0.1 to 0.9, in steps of 0.1. Simulation was conducted in each case. The simulation outcomes are given in table 4.2, along with the energy gap values of $Al_xGa_{1-x}As$ for different alloy compositions. Figures 4.1- 4.9 show the light J-V characteristics curves for all these simulations.

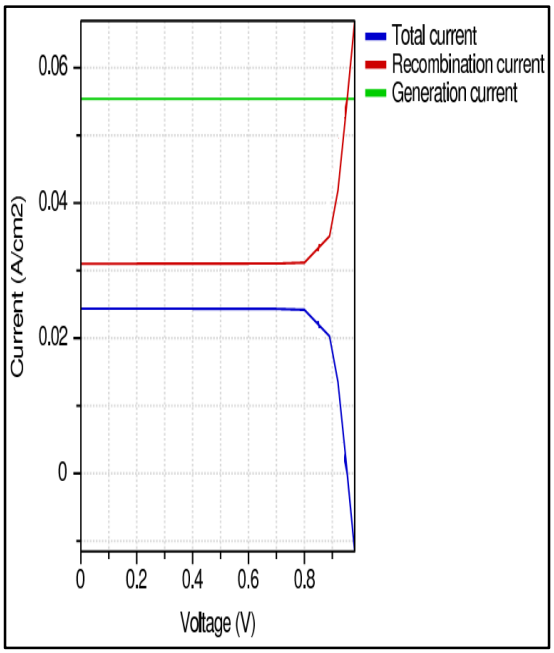

Fig. 4.1 Light J-V characteristics curve with x= 0.1 in $Al_xGa_{1-x}As$.

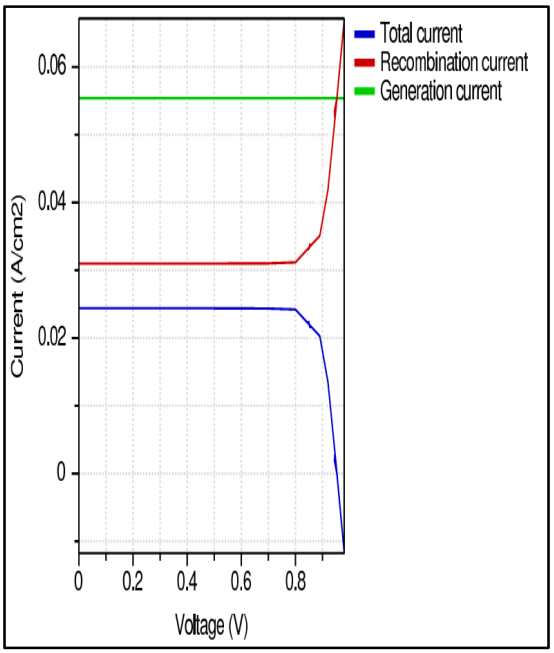

Fig. 4.3 Light J-V characteristics curve with x= 0.3 in $Al_xGa_{1-x}As$.

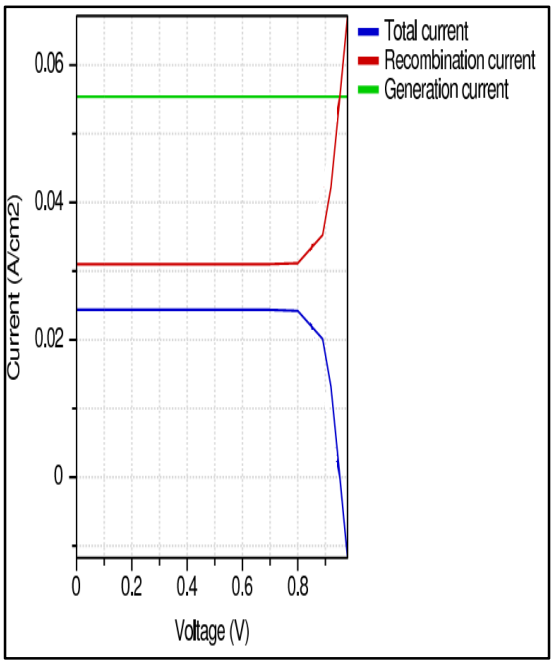

Fig. 4.2 Light J-V characteristics curve with x= 0.2 in $Al_xGa_{1-x}As$.

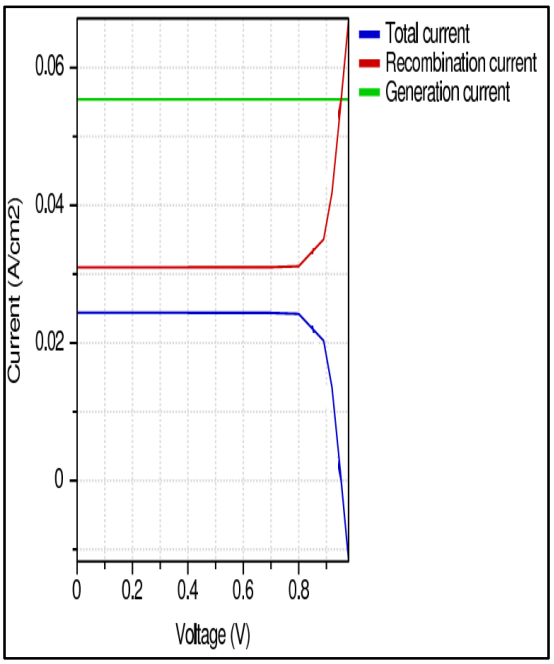

Fig. 4.4 Light J-V characteristics curve with x= 0.4 in $Al_xGa_{1-x}As$.

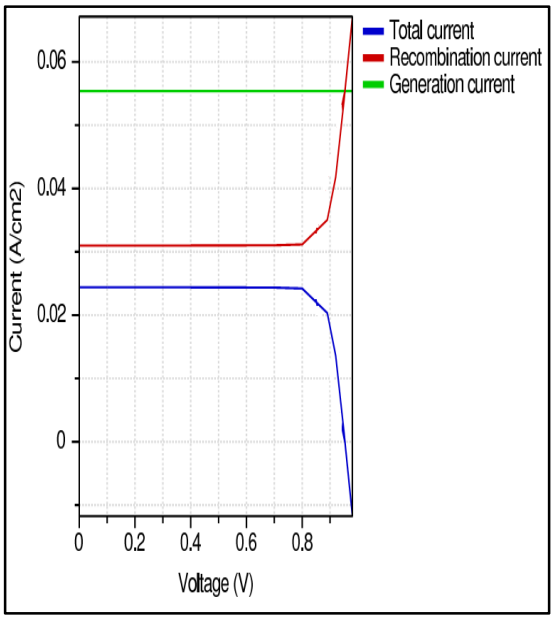

Fig. 4.5 Light J-V characteristics curve with x= 0.5 in $Al_xGa_{1-x}As$.

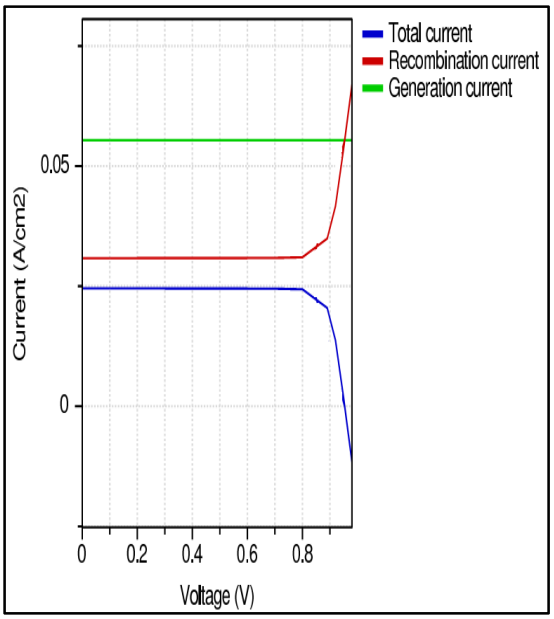

Fig. 4.7 Light J-V characteristics curve with x= 0.7 in $Al_xGa_{1-x}As$.

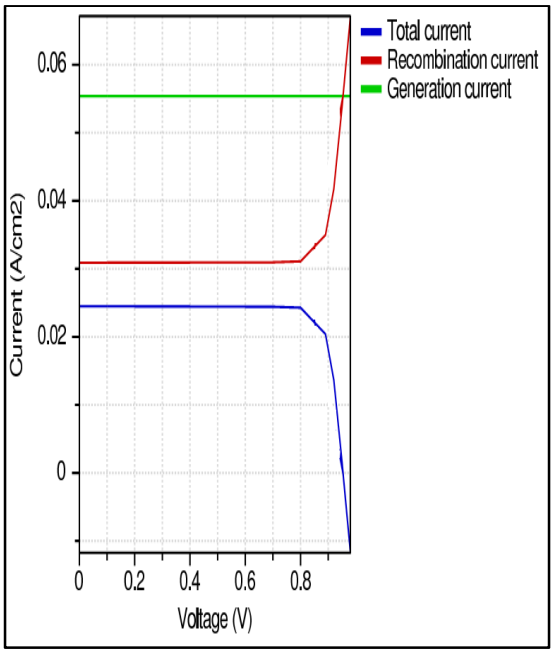

Fig. 4.6 Light J-V characteristics curve with x= 0.6 in $Al_xGa_{1-x}As$.

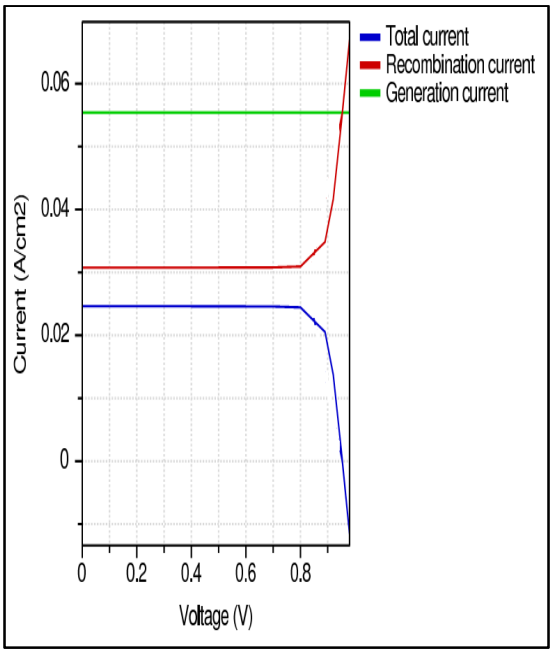

Fig. 4.8 Light J-V characteristics curve with x= 0.8 in $Al_xGa_{1-x}As$.

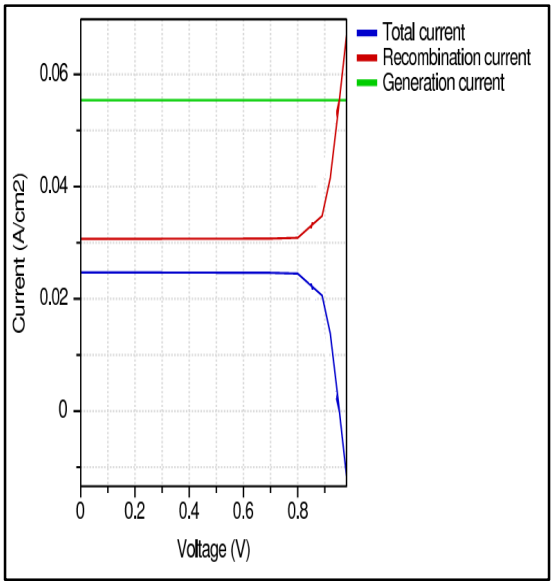

Fig. 4.9 Light J-V characteristics curve with x= 0.9 in $Al_xGa_{1-x}As$.

Now, efficiency (η) values from table 4.2 are plotted against corresponding values of x (Aluminium mole fraction). The resulting graph is shown in figure 4.10.

Table 4.2

Simulation Results for Different Alloy Compositions of Aluminium Gallium Arsenide

x in $Al_xGa_{1-x}As$	**Energy Gap (eV)**	**Jsc (mA/ cm^2)**	**Voc (V)**	**FF**	**η (%)**
0.1	1.55	24.38	0.9531	0.8777	20.39
0.2	1.67	24.39	0.9523	0.8777	20.39
0.3	1.8	24.41	0.9532	0.8777	20.42
0.4	1.92	24.41	0.9534	0.8778	20.43
0.5	1.998	24.41	0.9534	0.8778	20.43
0.6	2.03	24.48	0.9535	0.8778	20.49
0.7	2.06	24.56	0.9535	0.8778	20.56
0.8	2.09	24.64	0.9534	0.8778	20.62
0.9	2.13	24.70	0.9535	0.8778	20.67

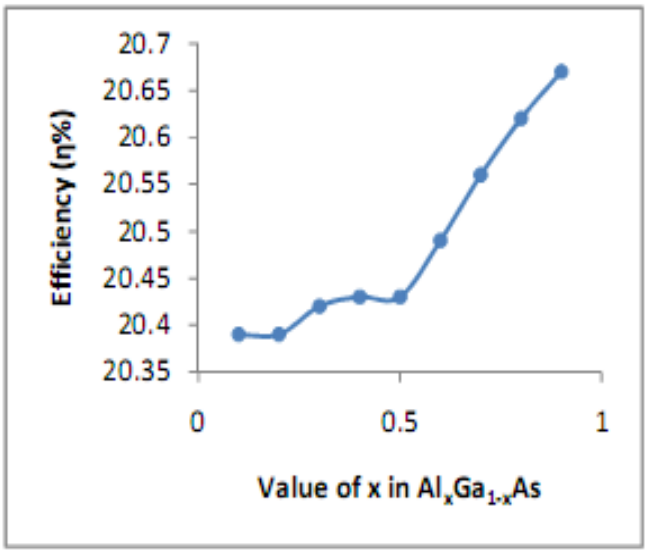

Fig. 4.10 Graph of efficiency versus Aluminium mole fraction in $Al_xGa_{1-x}As$.

The graph in figure 4.10 shows that higher efficiencies are obtained as the Aluminium mole fraction is increased in $Al_xGa_{1-x}As$. The top layer ($Al_xGa_{1-x}As$ layer) acts like a window layer [29] in the heterojunction solar cell, as mentioned in section 1.2. It is an established fact that the optical absorption in the base (absorber) layer increases with higher bandgap of the window layer material [8, 26]. Higher optical absorption leads to higher output current and, as a result, higher efficiency. Now, it is seen from table 4.2 that the bandgap of $Al_xGa_{1-x}As$ increases with increasing Aluminium mole fraction (x) in the alloy. So, the efficiency is supposed to increase with increasing values of x, which is supported by the graph in figure 4.10. So, in order to achieve high efficiency, Aluminium mole fraction in $Al_xGa_{1-x}As$ should be kept as high as possible. The irregularity in efficiency increment with increasing x is mainly due to the transition of $Al_xGa_{1-x}As$ from a direct to indirect material with increasing x [28].

4.6.2 **Varying Alloy Composition in $Al_xIn_{1-x}As$ (Middle Layer)**

Aluminium mole fraction (x) in $Al_xIn_{1-x}As$ was varied from 0.1 to 0.6, in steps of 0.1. The light J-V characteristics curves for x = 0.3- 0.6 are given in figures 4.11- 4.14. The simulation results are summarized in table 4.3. A plot of efficiency versus Aluminium mole fraction (x) in $Al_xIn_{1-x}As$ is given in figure 4.15. It is to be mentioned that simulations for x > 0.6 in $Al_xIn_{1-x}As$ were not conducted, because $Al_{0.7}In_{0.3}As$ has an indirect bandgap of 1.85 eV [38], which is far from the optimum bandgap (1.4 eV) for the absorber of a solar cell [11]. The bandgap becomes even higher for higher values of x.

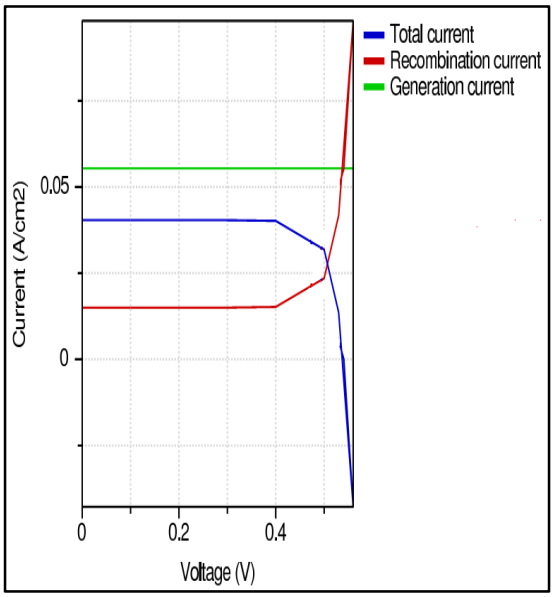

Fig. 4.11 Light J-V characteristics curve with x= 0.3 in $Al_xIn_{1-x}As$.

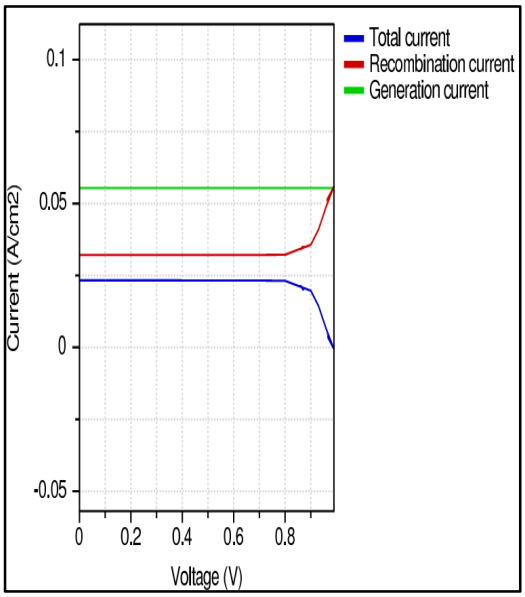

Fig. 4.13 Light J-V characteristics curve with x= 0.5 in $Al_xIn_{1-x}As$.

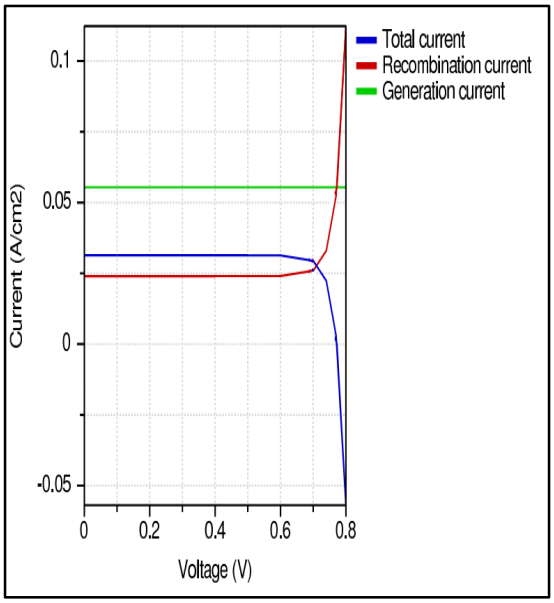

Fig. 4.12 Light J-V characteristics curve with x= 0.4 in $Al_xIn_{1-x}As$.

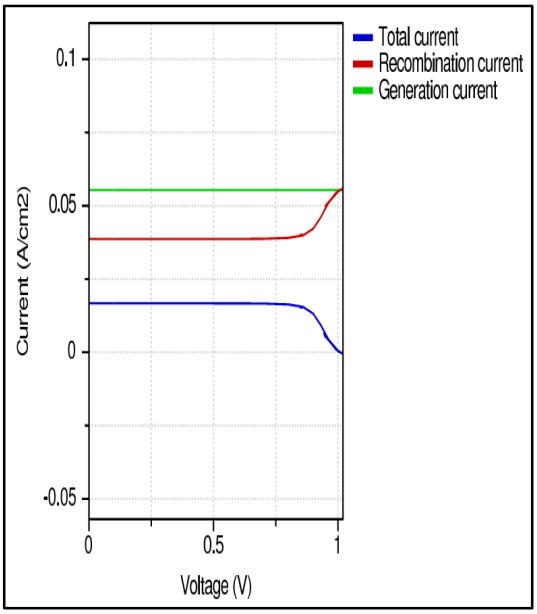

Fig. 4.14 Light J-V characteristics curve with x= 0.6 in $Al_xIn_{1-x}As$.

Table 4.3

Simulation Results for Different Alloy Compositions of Aluminium Indium Arsenide

x in $Al_xIn_{1-x}As$	**Energy Gap (eV)**	**Jsc (mA/ cm^2)**	**Voc (V)**	**FF**	**η (%)**
0.1	0.5	55.92	0.075	0.4136	1.73
0.2	0.75	47.14	0.3087	0.7264	10.57
0.3	1.0	40.4	0.5408	0.814	17.78
0.4	1.23	31.4	0.7726	0.8568	20.79
0.5	1.48	23.29	0.9867	0.8809	20.24
0.6	1.75	16.71	1.0043	0.8825	14.81

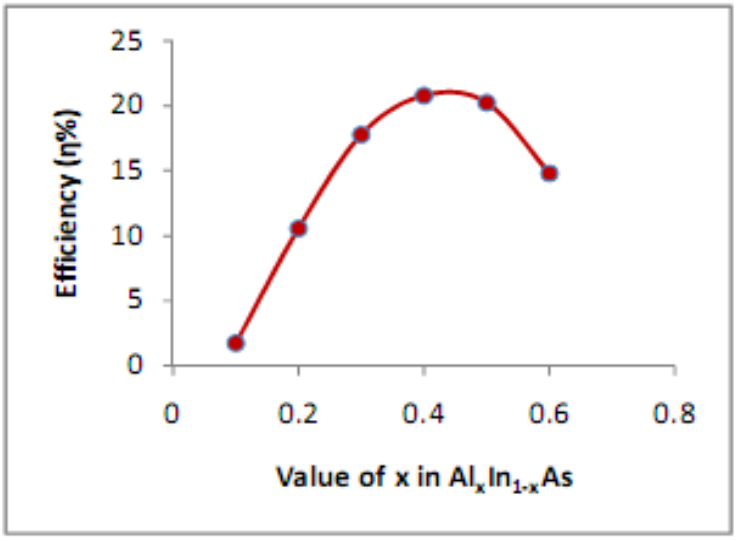

Fig. 4.15 Graph of efficiency versus Aluminium mole fraction in $Al_xIn_{1-x}As$.

The graph in figure 4.15 shows that the highest level of efficiency is obtained when Aluminium mole fraction in $Al_xIn_{1-x}As$ is between 0.4 and 0.5. So, the value of x in $Al_xIn_{1-x}As$ should be kept 0.4 ~ 0.5 for optimization.

4.6.3 **Varying Alloy Composition of $Ga_xIn_{1-x}As$ (Bottom Layer)**

Gallium mole fraction (x) in $Ga_xIn_{1-x}As$ was varied from 0.1 to 0.9, in steps of 0.1. The simulation outcomes are shown in table 4.4. Light J-V characteristics curves for these simulations are shown in figures 4.16- 4.24.

Table 4.4

Simulation Results for Different Alloy Compositions of Gallium Indium Arsenide

x in $Ga_xIn_{1-x}As$	Energy Gap (eV)	Jsc (mA/ cm^2)	Voc (V)	FF	η (%)
0.1	0.43	24.51	0.4347	0.783	8.34
0.2	0.50	24.51	0.5159	0.8076	10.21
0.3	0.59	24.51	0.6071	0.8289	12.33
0.4	0.68	24.52	0.7066	0.8469	14.67
0.5	0.78	24.53	0.8176	0.8627	17.3
0.6	0.89	24.55	0.9209	0.8745	19.77
0.7	1.01	24.56	0.9583	0.8782	20.67
0.8	1.14	24.59	0.9593	0.8783	20.72
0.9	1.28	25.2	0.9605	0.8785	21.26

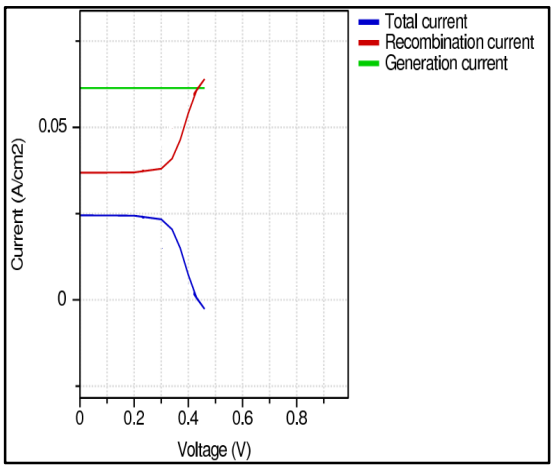

Fig. 4.16 Light J-V characteristics curve with x= 0.1 in $Ga_xIn_{1-x}As$.

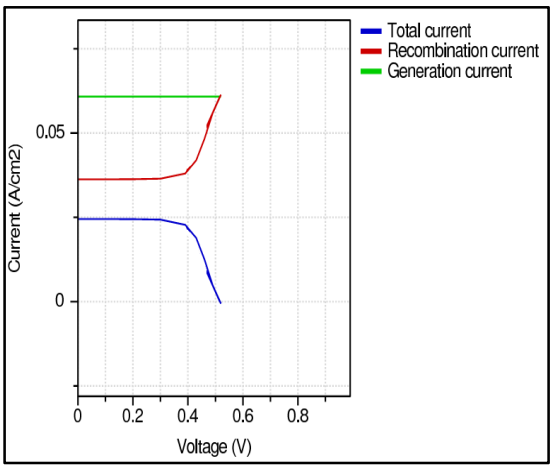

Fig. 4.17 Light J-V characteristics curve with x= 0.2 in $Ga_xIn_{1-x}As$.

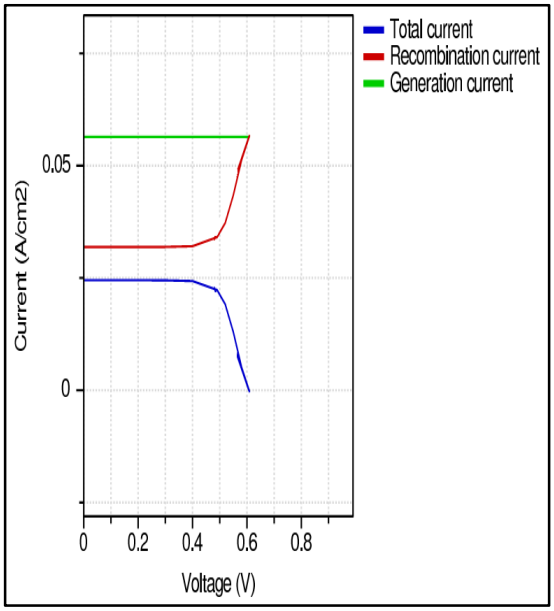

Fig. 4.18 Light J-V characteristics curve with x= 0.3 in $Ga_xIn_{1-x}As$.

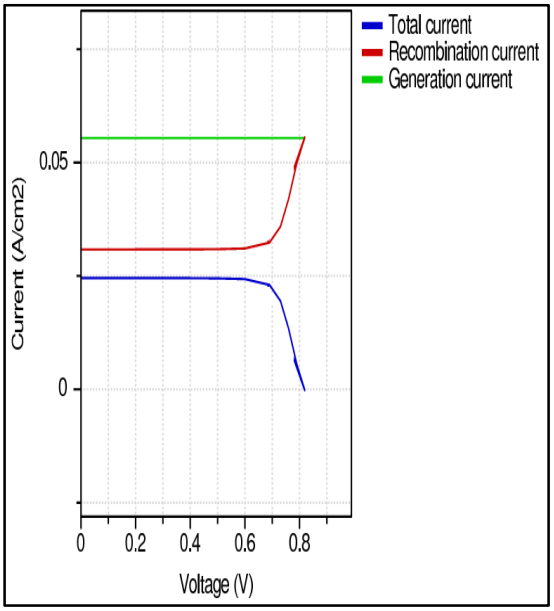

Fig. 4.20 Light J-V characteristics curve with x= 0.5 in $Ga_xIn_{1-x}As$.

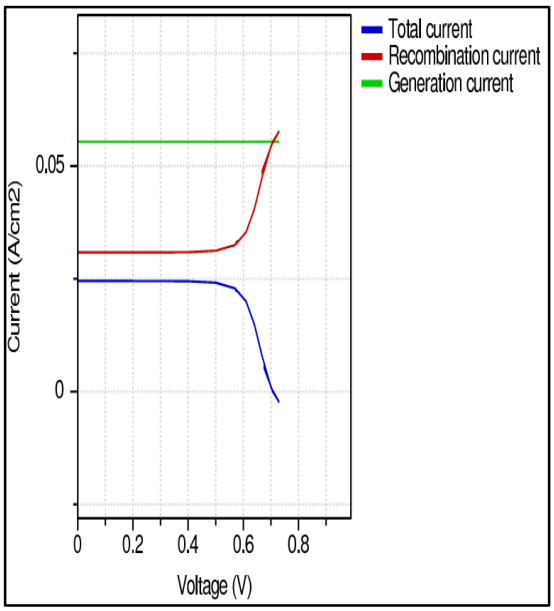

Fig. 4.19 Light J-V characteristics curve with x= 0.4 in $Ga_xIn_{1-x}As$.

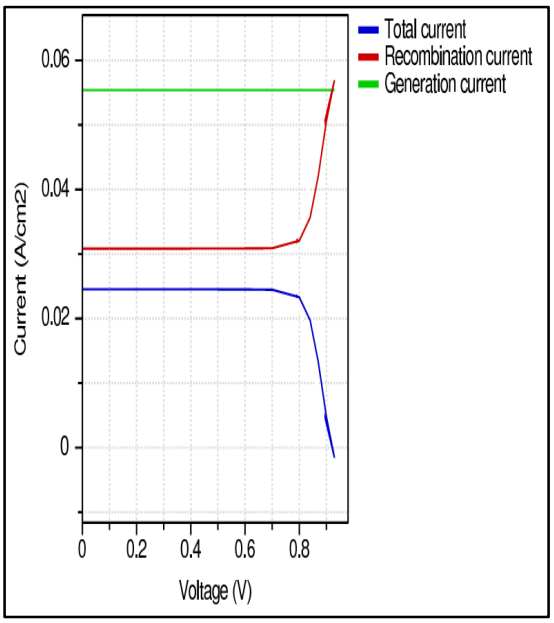

Fig. 4.21 Light J-V characteristics curve with x= 0.6 in $Ga_xIn_{1-x}As$.

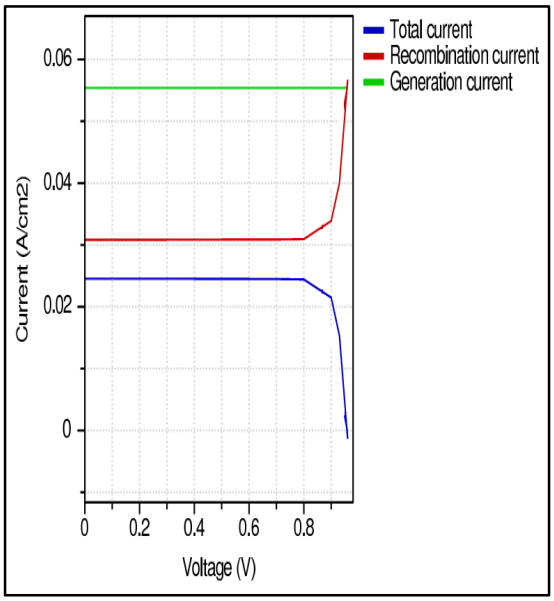

Fig. 4.22 Light J-V characteristics curve with x= 0.7 in $Ga_xIn_{1-x}As$.

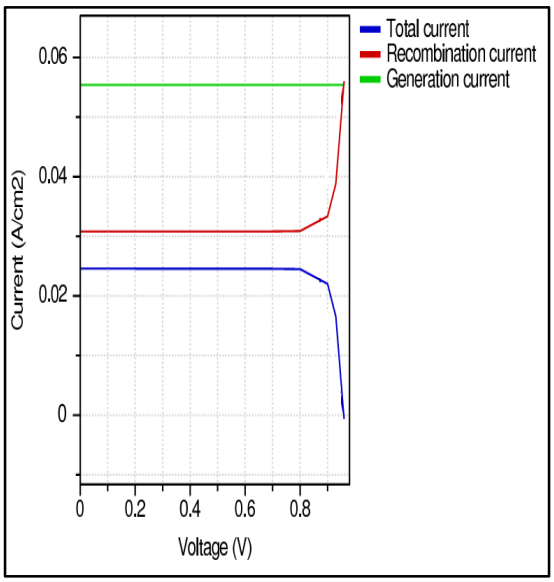

Fig. 4.23 Light J-V characteristics curve with x= 0.8 in $Ga_xIn_{1-x}As$.

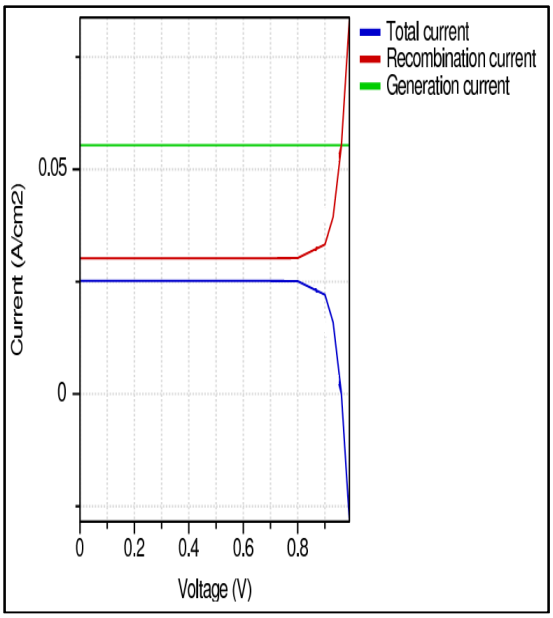

Fig. 4.24 Light J-V characteristics curve with x= 0.9 in $Ga_xIn_{1-x}As$.

Figure 4.25 gives a plot of efficiency versus Gallium mole fraction (x) in $Ga_xIn_{1-x}As$.

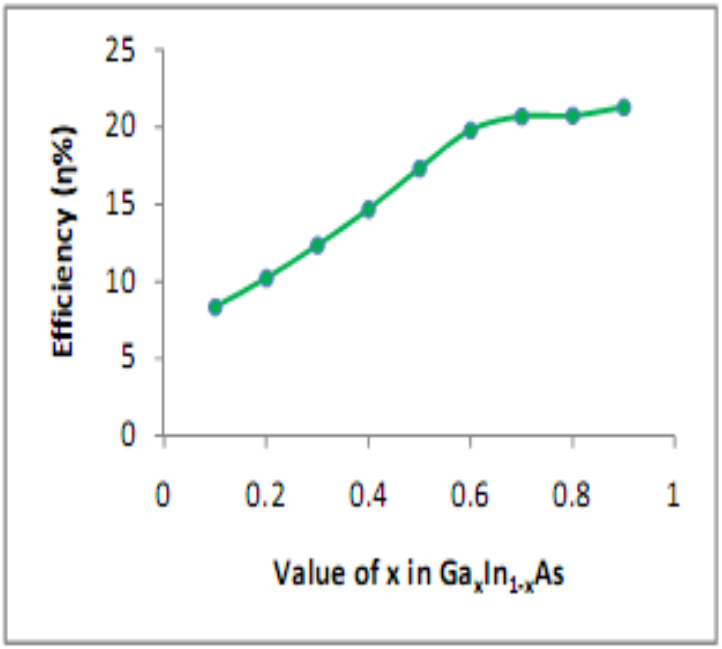

Fig. 4.25 Graph of efficiency versus Gallium mole fraction in $Ga_xIn_{1-x}As$.

It is evident from figure 4.25 that efficiency increases with increasing Gallium mole fraction in $Ga_xIn_{1-x}As$. Actually, the BSF layer plays little role in absorption, but the open-circuit voltage increases slightly with increasing bandgap of the BSF layer [43, 44], and so the efficiency. So, value of x in $Ga_xIn_{1-x}As$ should be kept high for optimization towards higher efficiency.

4.6.4 **Optimization of Alloy Composition**

4.6.4.1 First Design

From the analysis of the efficiency curves, it was evident that x value in $Al_xIn_{1-x}As$ should be taken around 0.4, while x values for $Al_xGa_{1-x}As$ and $Ga_xIn_{1-x}As$ should be taken as high as possible. From this insight, a design is proposed for the heterojunction solar cell. For this particular design, Aluminium mole fraction in $Al_xGa_{1-x}As$ is taken as 0.9. For the base layer material ($Al_xIn_{1-x}As$), the mole fraction of Aluminium is taken as 0.4. In $Ga_xIn_{1-x}As$ (Bottom layer material), the Gallium mole fraction is taken as 0.9. All other design parameters are kept

the same as listed in table 4.1. Figure 4.26 shows the light J-V characteristics graph obtained for this design.

From figure 4.26, the open-circuit voltage (V_{oc}) is found to be 0.7739 V. The short-circuit current density (J_{sc}) is pretty high (31.47 mA/cm^2), and the calculated fill factor is 0.8569. The calculated efficiency is 20.87%. It is to be noted that a higher efficiency value was obtained during Gallium mole fraction variation in $Ga_xIn_{1-x}As$ (at x= 0.9). So, clearly, this design does not give the best level of optimization.

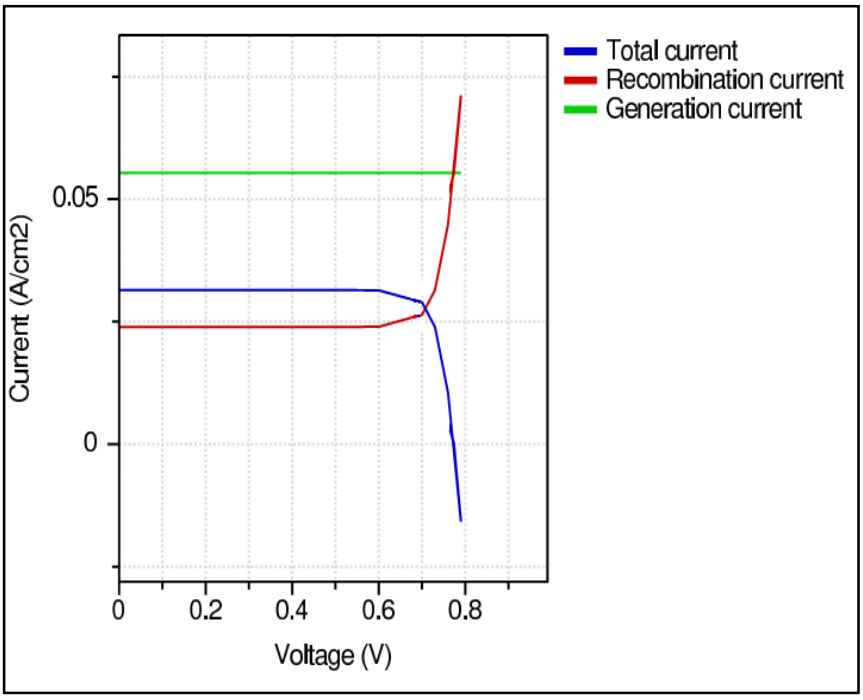

Fig. 4.26 Light J-V characteristics of the first design.

4.6.4.2 Second Design

In this design, Aluminium mole fraction in $Al_xIn_{1-x}As$ is taken as 0.5 (x= 0.5). Every other device parameter is kept the same as the first design. The light J-V characteristics graph obtained for this design is shown in figure 4.27.

From figure 4.27, values of the open-circuit voltage (V_{oc}) and the short-circuit current density (J_{sc}) are found as 1.0179 V and 23.72 mA/cm^2, respectively. Clearly, the voltage has increased,

but at the cost of a reduction in current. The calculated fill factor is 0.8837, and the resulting efficiency is 21.34%. So, the efficiency has increased as the Al mole fraction in $Al_xIn_{1-x}As$ is taken as 0.5.

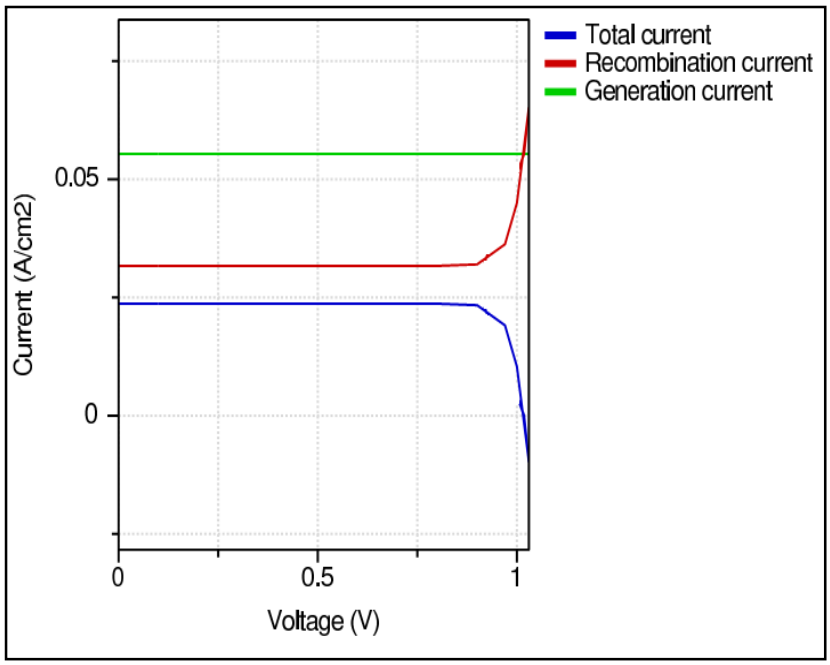

Fig. 4.27 Light J-V characteristics of the second design.

4.6.4.3 Third Design

In this design, Aluminium mole fraction in $Al_xIn_{1-x}As$ is taken as the default value (x= 0.48) listed in table 4.1. Every other device parameter is kept the same as the first design. Figure 4.28 shows the light J-V characteristics graph obtained for this design.

For the third design, the obtained open-circuit voltage is 0.9607 V, while the short-circuit current density is 25.34 mA/cm^2. The calculated fill factor is 0.8785. Finally, the calculated efficiency is 21.39%. This is the highest efficiency achieved from the three proposed designs.

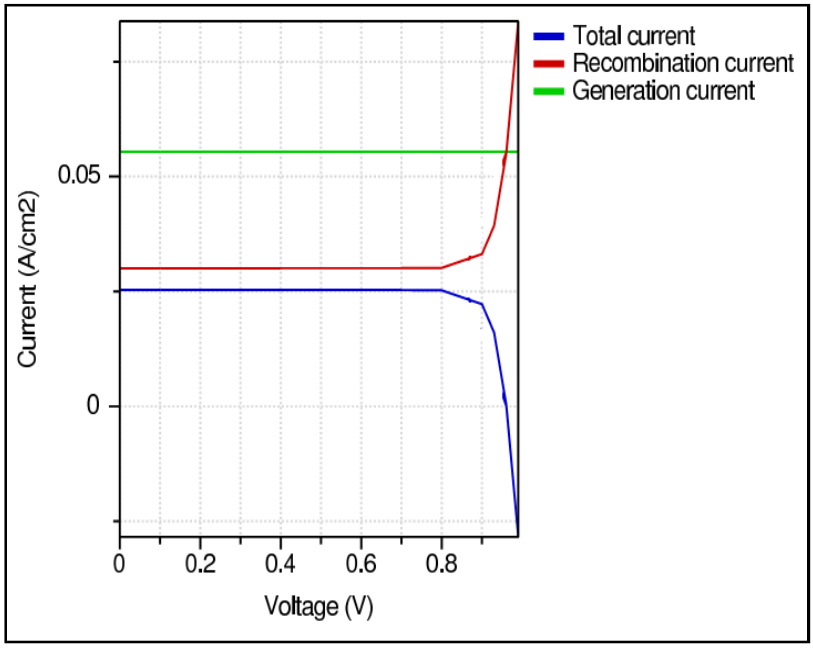

Fig. 4.28 Light J-V characteristics of the third design.

4.6.5 **Approach for Maximizing the Efficiency**

From the analysis of the efficiency variation curves and the outcomes of the proposed designs, it is obvious that in order to achieve the maximum possible efficiency from the $Al_xGa_{1-x}As$ /$Al_xIn_{1-x}As$ heterojunction solar cell, Aluminium mole fraction in $Al_xIn_{1-x}As$ should be kept somewhere between 0.4 and 0.5, while the Aluminium mole fraction in $Al_xGa_{1-x}As$ and Gallium mole fraction in $Ga_xIn_{1-x}As$ should be kept as high as possible. Inspecting the efficiency versus Aluminium mole fraction curve for $Al_xIn_{1-x}As$ more precisely suggests that the Aluminium mole fraction should be kept between 0.45 and 0.5. Simulations have been done for x values up to 0.9 in $Al_xGa_{1-x}As$ and $Ga_xIn_{1-x}As$, but the efficiency curves suggest that x values should be very close to 1 for achieving the highest possible efficiency with these materials.

Remarks

In this chapter, dependence of energy conversion efficiency on alloy composition has been investigated in details for the $Al_xGa_{1-x}As$ / $Al_xIn_{1-x}As$ heterojunction solar cell. Effect of change in alloy composition on efficiency has been analysed separately for each layer of the device. This

analysis will be helpful in selecting materials with optimum combination of bandgaps for fabricating heterojunction solar cells. The results found in this chapter can provide a better insight into the way of alloy composition optimization in heterojunction and multijunction solar cells fabricated from ternary and quaternary alloys for achieving the highest possible efficiency.

Chapter 5- Practical Solutions for Fabrication Purpose

5.4 Problems in the Proposed Designs

5.4.1 Lattice Mismatch

In the final best design proposed in section 4.3.4.3, $Al_{0.9}Ga_{0.1}As$, $Al_{0.48}In_{0.52}As$ and $Ga_{0.9}In_{0.1}As$ were taken as the top, middle and bottom layer materials, respectively. Substrate for the structure was Germanium (Ge). The major problem in this design is the high lattice mismatch between the layers. Germanium has a lattice constant of 5.65 Å [14]. Now, the growth of the BSF layer ($Ga_{0.9}In_{0.1}As$) on the substrate demands perfect lattice-matching between these two materials, so that the structure is defect-free [14]. But the lattice constant of $Ga_{0.9}In_{0.1}As$ is 5.6938 Å [28], which results in a lattice mismatch of 0.77% with Ge. Though the mismatch is small, it restricts the growth of $Ga_{0.9}In_{0.1}As$ on Ge to a critical layer thickness of around 12 nm [40].

$Al_{0.48}In_{0.52}As$ has a lattice constant of 5.8686 Å (lattice-matched with InP [26]). So, the lattice mismatch between $Ga_{0.9}In_{0.1}As$ and $Al_{0.48}In_{0.52}As$ is 2.98%, which is pretty high, and gives a critical layer thickness of 2 nm only [40].

$Al_{0.9}Ga_{0.1}As$ has a lattice constant of 5.66032 Å [28], and the lattice mismatch between $Al_{0.9}Ga_{0.1}As$ and $Al_{0.48}In_{0.52}As$ is 3.55%. This gives a critical layer thickness of around 2 nm for epitaxial growth [40].

This issue is of lattice mismatch is vital, as it determines whether the device can be fabricated to give optimum device performance or not. High defect density degrades the quality of the structure, and results in poor performance and device lifetime. The possible solutions to this problem have been discussed in section 5.2.1, with appropriate references.

5.4.2 High Fabrication Cost

The designs proposed in sections 3.2.7 and 4.3.4 yield nearly the maximum possible efficiency for this particular heterojunction solar cell, but the issue of materials and fabrication cost was not considered while proposing the designs. The only target there was to maximize the efficiency. But the fabrication cost of ternary III-V compounds is high [41], and bulk III-V solar cell is not a cost-effective option. So, the reduction of layer thickness is necessary for the proposed designs, especially for the absorber layer ($Al_{0.48}In_{0.52}As$), as it was kept very thick. A thicker absorber will surely absorb a greater number of photons, but there must be a trade-off between the desired efficiency and the material cost.

5.5 Practical, Cost-effective Designs

5.5.1 Solving the Lattice Mismatch Issue

One way to solve the lattice mismatch problem between two adjacent layers is to apply a buffer layer in between. The lattice constant of the buffer layer is intermediate to that of the two adjacent layers, and it helps to adjust the lattice mismatch to some extents. Now, it is easy to find a buffer layer for adjusting the lattice mismatch between the bottom layer and the substrate, as the mismatch is small. But the major problem is to find a material as the buffer layer in between the $Al_{0.48}In_{0.52}As$ and $Ga_{0.9}In_{0.1}As$ layers, because the $Al_{0.48}In_{0.52}As$ absorber must be sufficiently thick, and the defect-free growth of a thick $Al_{0.48}In_{0.52}As$ layer on a material requires perfect lattice-matching between them. The ideal lattice constant of a buffer layer that can be applied between $Al_{0.48}In_{0.52}As$ and $Ga_{0.9}In_{0.1}As$ is around 5.78 Å, which still generates 1.5% lattice mismatch with the $Al_{0.48}In_{0.52}As$ layer, and gives a critical thickness of around 7 nm only [40]. So, using a buffer layer between $Al_{0.48}In_{0.52}As$ and $Ga_{0.9}In_{0.1}As$ cannot be a solution.

We note from section 3.2.3 that an ultra-thin emitter layer improves the performance of the solar cell, as it acts as a window layer for the cell. This is why we used a 10 nm $Al_{0.9}Ga_{0.1}As$ layer in our final optimized design in section 4.3.4. The results in section 3.2.3 indicate that window layers thinner than 10 nm will give even better performance. So, we do not actually need any buffer layer between $Al_{0.9}Ga_{0.1}As$ and $Al_{0.48}In_{0.52}As$, rather we can go for an ultra-thin window layer which has a thickness equal to the critical layer thickness in this case (2 nm).

Growth of a 2 nm layer can be done by e-beam evaporation (e-beam evaporators today can offer a deposition rate of 0.5 nm/ min or even less [42]), or some other deposition method that can provide low deposition rate.

Now, we are back to the problem of lattice mismatch between $Al_{0.48}In_{0.52}As$ and $Ga_{0.9}In_{0.1}As$. As we have already discussed that the growth of a buffer layer is not a feasible idea, we move on to a new approach. We note that the lattice constant of $Ga_{0.9}In_{0.1}As$ can be changed if we change the alloy composition of the material, and $Ga_{0.47}In_{0.53}As$ is perfectly lattice matched to $Al_{0.48}In_{0.52}As$ [27, 28]. Now, section 4.3.3 suggests that reducing the Gallium mole fraction in $Ga_{0.47}In_{0.53}As$ degrades the efficiency of the solar cell; yet we have to follow this approach to ensure perfect lattice matching between the absorber and the BSF layer, so that the absorber can be grown in any desired thickness. So, we will be using $Ga_{0.47}In_{0.53}As$ as the BSF layer material in our practical designs, which will be proposed in section 5.2.2. We note that $Ga_{0.47}In_{0.53}As$ has a direct bandgap of 0.7734 eV, which is less than that of $Ga_{0.9}In_{0.1}As$ (1.28 eV). This will reduce the open-circuit voltage of the device, which will reduce the efficiency, as discussed in section 4.3.3.

A new problem arises that the lattice mismatch between $Ga_{0.47}In_{0.53}As$ and Ge is higher (3.7%) than it was for $Ga_{0.9}In_{0.1}As$. This gives a critical layer thickness for the growth of $Ga_{0.47}In_{0.53}As$ on Ge of slightly less than 2 nm [40]. This means that we should not allow the growth of > 2 nm thick $Ga_{0.47}In_{0.53}As$ epitaxial layer on Ge substrate. We observed in section 3.2.1 that the change of efficiency with changing BSF layer thickness is insignificant. However, we did not investigate this effect for thickness < 200 nm. Ultra-thin BSF layers may have significant impact on efficiency.

5.5.2 Cost Effective Solar Cell- a Thin Film Approach

As we mentioned in section 5.1.2, a trade-off is needed to be made between cell efficiency and material cost. We have already decided to use 2 nm thick emitter layer and BSF layer in the solar cell, for eliminating the effect of lattice mismatch. So, we bring back the highest efficiency design discussed in section 4.3.4.3, with three modifications- using $Ga_{0.47}In_{0.53}As$, instead of

$Ga_{0.9}In_{0.1}As$ for the BSF layer; changing the top layer thickness to 2 nm, and changing the BSF layer thickness to 2 nm. Figure 5.1 shows the J-V characteristics curve for this design.

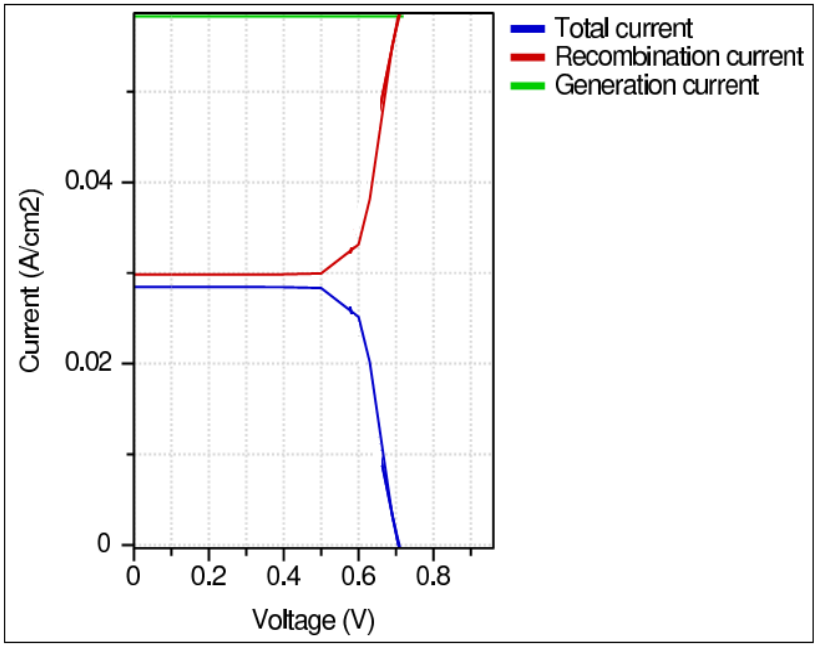

Fig. 5.1 Light J-V characteristics curve for the design of section 4.3.4.3 after modification.

The short-circiut current density for this design is 28.47 mA/ cm^2, open-circuit voltage is 0.7063 V, and the fill factor (FF), calculated using equation (6) is 0.8469. The calculated efficiency is 17.03%. We can see that the efficiency has decreased significantly, compared to the 21.39% efficiency in section 4.3.4.3, due to the reasons already discussed.

Now, we have conducted a number of simulations with varying base layer thickness values, in order to give us a good number of options for the efficiency and cost trade-off. Table 5.1 lists the simulation outcomes. A graph of efficiency versus middle layer thickness of the modified design is shown in figure 5.2.

The results shown in table 5.1 give few good design options that are cost-effective and moderately efficient. It is to be noted that thickness of the emitter and base (2 nm each) are negligible, when the base thickness is in the range of microns. So, we can consider the base thickness as the thickness of the cell (excluding the substrate thickness).

Table 5.1
Simulation Results for Varying Base Thickness of the Modified Design

Base Thickness (µm)	**V_{oc} (V)**	**J_{sc} (mA/cm^2)**	**FF**	**Efficiency (η%)**
100	0.7063	28.47	0.8469	17.03
20	0.6419	28.33	0.8357	15.2
10	0.6208	28.13	0.8317	14.52
5	0.6004	27.66	0.8275	13.74
2	0.5706	25.95	0.821	12.16

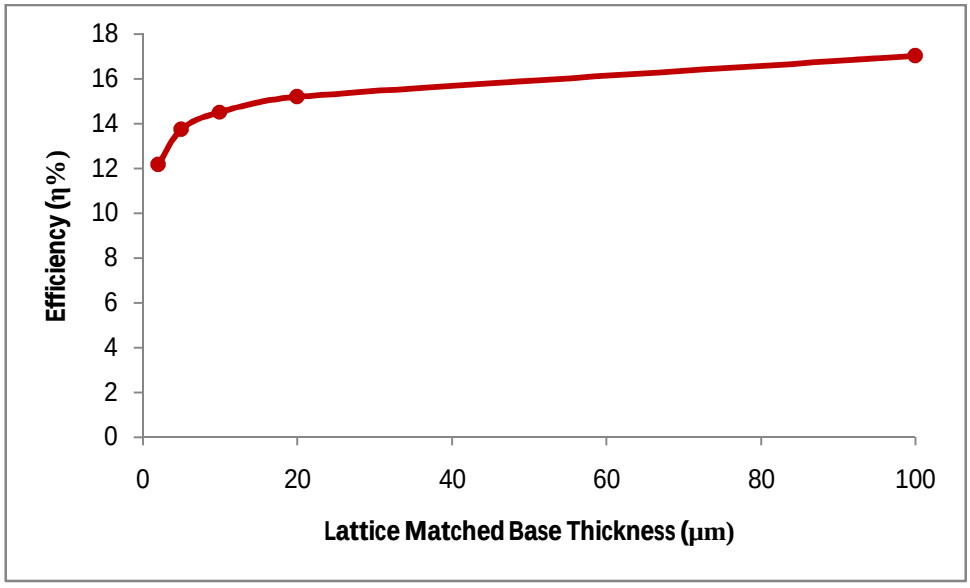

Fig. 5.2 Efficiency vs absorber thickness of the modified design.

We see from table 5.1, that a 10 µm thick cell yields an efficiency of 14.52%. The 5 µm cell can be an option for a thin film solar cell, which yields an efficiency of 13.74%. As a better thin film approach, we can consider the 2 µm cell (starting point of the graph), which gives an efficiency of 12.16%. The light J-V characteristics curve for the 2 µm cell is given in figure 5.3.

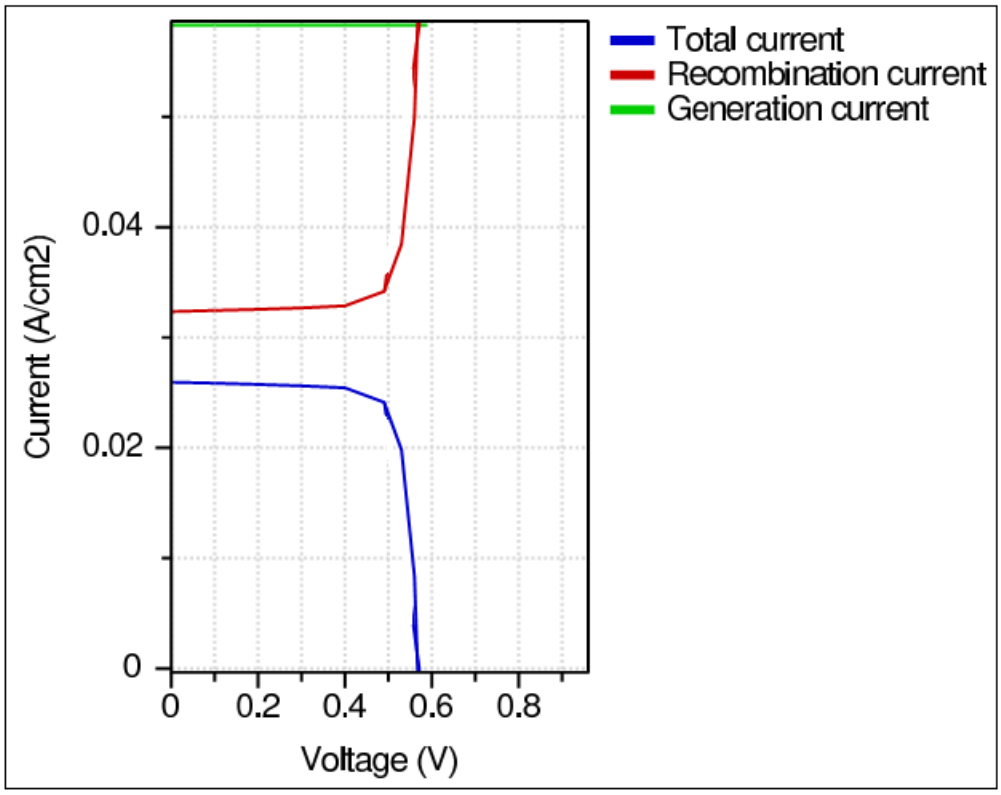

Fig. 5.3 Light J-V characteristics curve for 2 µm cell thickness (excluding substrate thickness).

5.5.3 About Substrate Doping

We can fabricate the device on Germanium wafer; the wafer being heavily p-doped (1×10^{18} cm^{-3}). One way to do this is to dope during crystal growth from the ingot. Heavily doped wafers are supposed to improve the solar cell performance to some extents [45].

5.5.4 About p-type Doping in $Al_{0.48}In_{0.52}As$

$Al_{0.48}In_{0.52}As$ is a less-investigated material for application in optoelectronic devices. So, we need to discuss about the realization of p-type doping in $Al_{0.48}In_{0.52}As$. $Al_{0.48}In_{0.52}As$ has an intrinsic carrier concentration of 1.6×10^{7} cm^{-3} (at 300 K) [46]. The electron affinity of $Al_{0.48}In_{0.52}As$ is 4.03 eV [47], which is moderate, and the material can be easily p-doped. Actually, both p-doping and n-doping are possible for $Al_{0.48}In_{0.52}As$, which is supported by previous works [25, 26, 48]. $Al_{0.48}In_{0.52}As$ p-n homojunction has been implemented very recently in thin film solar cells [25, 26].

5.6 A Better Approach

In the proposed cost-effective designs in section 5.2.2, we noticed that the efficiency has decreased, compared to the design in section 4.3.4.3, after using a $Ga_{0.47}In_{0.53}As$ BSF layer (which is lattice-matched to $Al_{0.48}In_{0.52}As$). This is mainly due to the low bandgap of $Ga_{0.47}In_{0.53}As$ (0.7734 eV), compared to that of $Ga_{0.9}In_{0.1}As$ (1.28 eV); this low bandgap degrades the open-circuit voltage of the solar cell drastically, as seen from table 5.1. The point is, if we use a $Ga_xIn_{1-x}As$ BSF layer, the x value must be kept at 0.47, for the growth of an $Al_{0.48}In_{0.52}As$ absorber on $Ga_xIn_{1-x}As$. The absorber must have a moderate thickness (which was 2 µm in our thin film design). So, the necessity of perfect lattice matching between the two materials ($Al_{0.48}In_{0.52}As$ and $Ga_xIn_{1-x}As$) cannot be compromised. So, in order to improve the output characteristics, we suggest the use of an InP substrate, instead of Ge. It is to be noted that InP is perfectly lattice-matched to $Al_{0.48}In_{0.52}As$ and $Ga_{0.47}In_{0.53}As$. Though InP is costlier than Ge [49], using InP for our solar cell is advantageous for two reasons- InP has a much higher bandgap (1.344 eV) than Ge, which improves the open-circuit voltage slightly; and the BSF layer can now be grown at any desired thickness. An ultra-thin BSF layer slightly degrades the efficiency of the cell, as previously mentioned.

Considering the issue of cost-effectiveness, we suggest our very final design of a thin film solar cell, where the $Al_{0.48}In_{0.52}As$ absorber is 2 µm thick, and the $Ga_{0.47}In_{0.53}As$ BSF layer has a thickness of 1 µm. The solar cell will be grown on InP substrate, instead of Ge. Every other design parameter is kept the same as the 2 µm solar cell, discussed in section 5.2.2. Simulation was conducted for this cell, and the light J-V characteristics curve is given in figure 5.4.

We note that this new thin film solar cell has a total thickness of 3 µm (excluding the substrate thickness). The short-circuit current density (J_{sc}) was obtained as 26.03 mA/cm^2, the open-circuit voltage being 0.637 V, and the fill factor (FF) being 0.8348. The efficiency is calculated as 13.84%. We see, with this design, the open-circuit voltage is considerably improved, and so the efficiency.

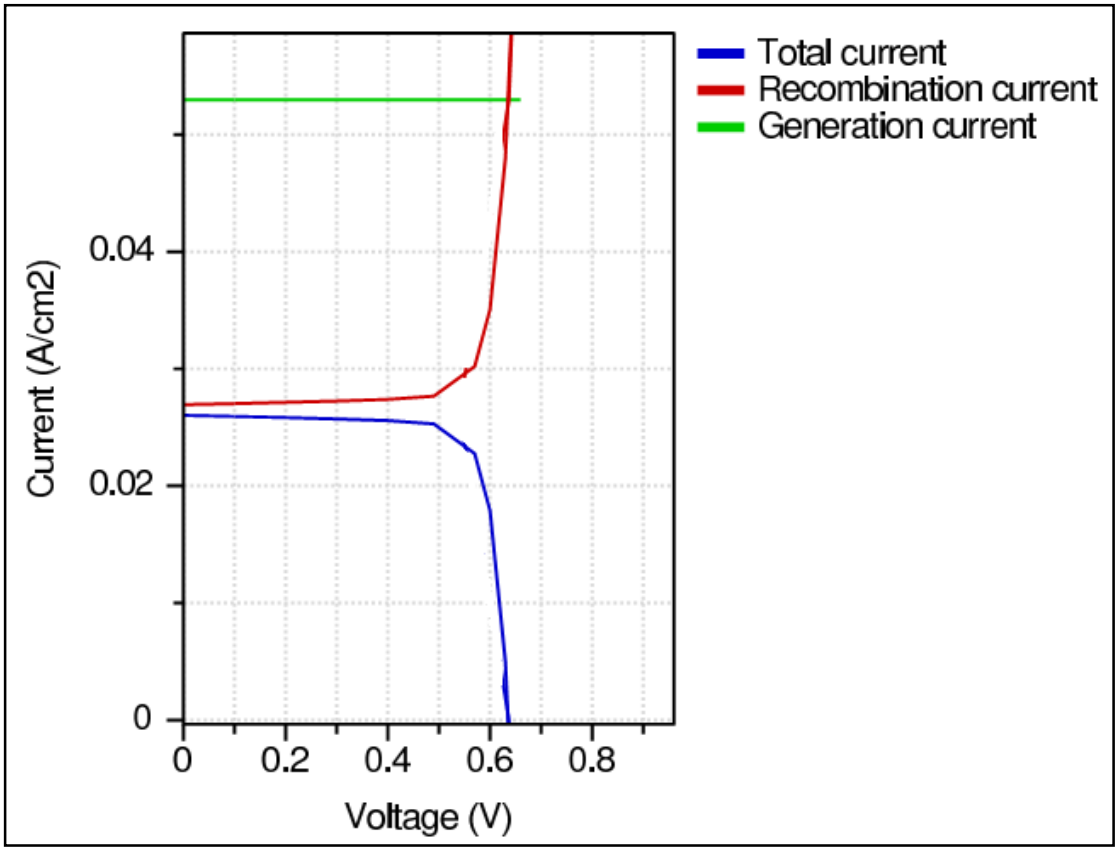

Fig. 5.4 Light J-V characteristics curve for the 3 μm cell on InP substrate.

Remarks

This chapter discusses in details the critical fabrication issues of our proposed solar cell, and proposes more practical and cost-effective designs. One significant contribution made in this chapter is the design of a thin film solar cell with our initial cell structure and materials. Finally, the substrate was changed to InP from Ge, which gave more improved results.

Chapter 6- Summary

6.4 Overview of the Work

In chapter 1, we have discussed the basic operational principles of solar cells, along with the basics of heterojunction solar cells. We have also discussed the application of III-V compounds in solar cells, with an investigation into the high-cost issue of III-V solar cells, which is the limiting factor for the mass fabrication of these solar cells. We have also given a brief outline of our research, and discussed the novelty in our device with appropriate references.

In chapter 2, we have introduced an initial design of an $Al_{0.7}Ga_{0.3}As/Al_{0.48}In_{0.52}As$ heterojunction solar cell, with its corresponding light J-V characteristics curve. Later, we have added a $Ga_{0.67}In_{0.33}As$ Back Surface Field (BSF) layer in the solar cell, which greatly improved the output characteristics of the solar cell.

In chapter 3, we have done detailed analysis for design optimization in the solar cell. We have optimized the layer thickness and doping concentration in each layer for high efficiency. We have separately investigated the effect of change in a particular design parameter on the efficiency of the cell, and analysed the outcomes with proper explanation of the underlying physics. We have also proposed two high efficiency designs.

In chapter 4, we have investigated the change in output characteristics of the device with varying alloy composition of the layer materials. Analysis was done separately for each layer material, to understand the effects more appropriately. The outcomes have been discussed, and the way of optimization of alloy composition at different layers was illustrated. Finally, we have proposed three high efficiency designs at the end of the chapter.

Up to chapter 4, the only target was to optimize the design parameters and material properties for achieving maximum efficiency. The proposed designs achieved pretty high efficiency values, but they were not investigated from the point of view of fabrication and cost-effectiveness.

Chapter 5 discusses these issues in details with practical solutions. This chapter discusses the critical issues of fabrication, and brings necessary modifications in the designs of chapter 3 and 4 accordingly. Trade-off between cost and efficiency was done, and moderate efficiency values were reported for practical, low-cost designs. A thin film approach was taken in the end, and the resulting output characteristics curves have been discussed.

6.2 Major Contributions of the Work

The most important contribution of this research work is the **introduction of an $Al_xGa_{1-x}As$ / $Al_xIn_{1-x}As$ heterojunction as the working p-n junction of a solar cell**. $Al_xIn_{1-x}As$ is a less investigated material as the constituent of a solar cell, and **it has only been tried in homojunction solar cells very recently** [25, 26]. **The advantage of forming a heterojunction of $Al_{0.48}In_{0.52}As$ with a high bandgap material is that, while $Al_{0.48}In_{0.52}As$ functions as the absorber of the cell ($Al_{0.48}In_{0.52}As$ has a direct bandgap of 1. 47 eV, which is near the optimum bandgap of 1.4 eV for the absorber of a solar cell [11]), the high bandgap upper layer can act as a window layer for the cell. This eliminates the necessity of a separate window layer.** Now, what opposes the realization of $Al_{0.48}In_{0.52}As$ in a useful heterojunction is the unavailability of a high bandgap material with a Zincblende structure, and the same lattice constant as $Al_{0.48}In_{0.52}As$. $Al_{0.9}Ga_{0.1}As$ has a lattice mismatch of 3.55% with $Al_{0.48}In_{0.52}As$. Lattice mismatch limits the growth of the upper $Al_{0.9}Ga_{0.1}As$ window layer on $Al_{0.48}In_{0.52}As$ to a very small critical thickness (≈ 2 nm) [40]. Now, **we have shown in our work (in section 3.2.3) that the efficiency is improved with an ultra-thin (few nanometers thick) window layer. We have also given the evidence of realization of very low deposition rates (0.5 nm / min or less) [42], which makes it possible to grow epitaxial layers which are only 2- 10 nm thick. So, it is possible to grow an ultra-thin (≈ 2 nm) window layer of $Al_{0.9}Ga_{0.1}As$ on $Al_{0.48}In_{0.52}As$. This implies that an $Al_{0.48}In_{0.52}As$/ $Al_{0.9}Ga_{0.1}As$ heterojunction is implementable, and it gives improved performance for our particular device, as the bandgap of the window material ($Al_{0.9}Ga_{0.1}As$) is high (2.13 eV).**

Another contribution of the work is the **investigation into the output characteristics of the solar cell with $Ga_{0.47}In_{0.53}As$ (lattice matched to $Al_{0.48}In_{0.52}As$) being applied as a back**

surface field (BSF) layer. Another outcome of the work is the **evidence of superiority of InP over Ge as a substrate for this particular solar cell.**

The works done in chapter 3 and 4 provide **useful insights into the optimization of design parameters and material properties for maximizing the efficiency level** in III-V solar cells.

6.3 Future Work

It is already mentioned that while using an $Al_{0.48}In_{0.52}As$ absorber, it is advantageous to use a heterojunction instead of a homojunction, because this gives the option to use a high bandgap window layer as part of the p-n junction. In our final design, $Al_{0.9}Ga_{0.1}As$ was used as the window layer, which has an indirect bandgap of 2.13 eV. This is a pretty good choice, provided that we choose our window layer material from the III-V compounds. But actually, a window layer with bandgap higher than 2.5 eV will significantly improve the efficiency. Unfortunately, if we restrict our choice to those III-V compounds which have a maximum of 4% lattice mismatch (critical layer thickness of ≈ 1.2 nm) with $Al_{0.48}In_{0.52}As$, we do not have many options that give a high bandgap. It is to be noted that GaP and $Ga_xIn_{1-x}P$ with $x \approx 0.9$, have bandgap between 2.2-2.26 eV [28], but they have a lattice mismatch of around 7%, with $Al_{0.48}In_{0.52}As$. For < 4% lattice mismatch, we can choose AlAs (3.55% lattice mismatch) from the binary compounds, or $AlAs_{0.9}Sb_{0.1}$ (2.8% lattice mismatch) or $AlP_{0.65}Sb_{0.35}$ (2.9% lattice mismatch) from the ternary compounds, or $Al_{0.75}Ga_{0.25}P_{0.7}Sb_{0.3}$ (3.7% lattice mismatch) from the quaternary compounds, which provide bandgaps of 2.16, 2.08, 2.1 and 2.1 eV, respectively [14, 50]. Looking at these bandgap values, we can conclude that we do not have much better options than $Al_{0.9}Ga_{0.1}As$ from the III-V compounds to use as a window layer.

If the window layer is chosen from II-VI compounds, which have a Zincblende lattice, then we may have better options, like ZnSe (3.37% lattice mismatch with $Al_{0.48}In_{0.52}As$, bandgap of 2.7 eV) or ZnTe (3.81% lattice mismatch with $Al_{0.48}In_{0.52}As$, bandgap of 2.25 eV). These materials can be worked out in future to replace $Al_{0.9}Ga_{0.1}As$ in our proposed heterojunction solar cell for higher efficiency.

Another development that can be done in our solar cell is to eliminate the $Ga_{0.47}In_{0.53}As$ BSF layer from the final design of section 5.3. Since the InP substrate is heavily ($\approx 10^{18}$ cm^{-3}) doped, it can work as a BSF layer in absence of the $Ga_{0.47}In_{0.53}As$ layer (the reader is requested to refer to section 2.1.1 for the functional principle of the BSF layer). This will not change the results of section 5.3 significantly. As the substrate is very heavily doped with respect to the $Al_{0.48}In_{0.52}As$ absorber, it can effectively function as a BSF layer. So, we can have a thin film solar cell which is only 2 μm thick (excluding substrate thickness), and yet yield an efficiency of nearly 14%.

The solar cell introduced in this work does not have an anti-reflective (AR) coating to reduce photon loss due to reflection, or a bragg reflector that would increase the quantum efficiency of the cell. Including such layers in the solar cell would give higher efficiency.

Bibliography

1. Peter Gevorkian, *Sustainable energy systems engineering: the complete green building design resource*, p. 498, McGraw-Hill Professional, New York, USA, 2007, ISBN: 978-0071473590.

2. Marius Grundmann, *The Physics of Semiconductors: An Introduction Including Nanophysics and Applications*, 2nd ed., p. 3, Springer-Verlag, Berlin, Germany, 2010, ISBN: 978-3642138843.

3. K. A. Tsokos, *Physics for the IB Diploma*, 5th ed., Cambridge University Press, Cambridge, UK, 2008, ISBN: 978-0521708203.

4. Urjart. (2008) Solar Cell: Basic Principle of Operation. [Online]. Available: http://urjart.wordpress.com/2008/10/05/solar-cell-%E2%80%93-basic-principle-of-operation/

5. M. A. Green, "Solar cell fill factors: General graph and empirical expressions," *Solid-State Electronics*, vol. 24, no. 8, pp. 788-789, 1981.

6. Zh. I. Alferov, "Heterostructures and their applications in optoelectronics", *Akademiia Nauk SSSR*, vol. 7, pp. 28-40, 1976.

7. Stephen J. Fonash, *Solar Cell Device Physics*, 2nd Ed., Academic Press, Elsevier, Massachusetts, USA, 2010, ISBN: 978-0123747747.

8. U. S. Department of Energy. (2011) Energy Basics. [Online]. Available: http://www.eere.energy.gov/basics/renewable_energy/pv_cell_structures.html

9. Peter Wurfel, *Physics of Solar Cells: From Principles to New Concepts*, Wiley-VCH Verlag GmbH & Co. KGaA, Weinheim, Germany, 2005, ISBN: 3-527-40428-7

10. L. J. A. Koster, E. C. P. Smits, V. D. Mihailetchi, and P. W. M. Blom, "Device model for the operation of polymer/fullerene bulk heterojunction solar cells", *Physical Review B*, vol. 72, pp. 085205-1 - 085205-9, 2005, DOI: 10.1103/PhysRevB.72.085205

11. T. Tiedje, E. Yablonovitch, G. D. Cody, and B. G. Brooks, "Limiting efficiency of Silicon solar cells", *IEEE Transactions on Electron Devices*, vol. ED-31, pp. 711-716, 1984.

12. L.W. James, "III-V Compound heterojunction solar cells", in *Proceedings of IEEE International Electron Devices Meeting*, vol. 21, pp. 87-90, Washington, USA, 1975.

13. J.E. Sutherland, and J.R. Hauser, "Optimum bandgap of several III–V heterojunction solar cells", *Solid-State Electronics*, vol. 22, no. 1, pp. 3-5, 1979.

14. B. G. Streetman, and S. K. Banerjee, *Solid State Electronic Devices*, 6th Ed., Prentice-Hall Inc., New Jersey, USA, 2006, ISBN: 978-8120330207.

15. M. A. Green, K. Emery, Y. Hishikawa, W. Warta, and E. D. Dunlop, "Solar cell efficiency tables (version 39)", *Progress in Photovoltaics: Research and Applications*, vol. 20, pp. 12-20, 2012.

16. F. Dimroth, "High-efficiency solar cells from III-V compound semiconductors", *Physica Status Solidi (c)*, vol. 3, no. 3, pp. 373-379, 2006.

17. B. Garcia, Jr., "Indium Gallium Nitride Multijunction Solar Cell Simulation Using Silvaco Atlas", M. Sc. Thesis, Naval Postgraduate School, Monterey, California, June 2007.

18. M. Meyer, and R.A. Metzger, “Flying high: The Commercial Satellite Industry Convert to Compound Semiconductor Solar Cells”, Compound Semiconductor, vol. 2, no. 6, pp. 22-24, 1996.

19. J.J. Schermer, G.J. Bauhuis, P. Mulder, E.J. Haverkamp, J. van Deelen, A.T.J. van Niftrik, and P.K. Larsen, “Photon confinement in high-efficiency, thin-film III–V solar cells obtained by epitaxial lift-off”, *Thin Solid Films,* vol. 511, pp. 645 – 653, 2006.

20. T.V. Torchynska, and G.P. Polupan, “III-V material solar cells for space application”, *Semiconductor Physics, Quantum Electronics & Optoelectronics,* vol. 5, no. 1, pp. 63-70, 2002.

21. A. Goetzberger, C. Heblinga, and H. Schockb, “Photovoltaic materials, history, status and outlook”, *Materials Science and Engineering: R: Reports,* vol. 40, no. 1, pp. 1-46, 2003.

22. J. L. Gray and Michael McLennan. (2008) Adept. [Online]. Available: http://nanohub.org/resources/adept/

23. A. S. Brown, U. K. Mishra, J. A. Henige, and M. J. Delaney, Journal of Vacuum Science & Technology B, vol. 6, no. 2, pp. 678-681, 1988.

24. L. Ajili, G. Scalari, N. Hoyler, M. Giovannini, and J. Faist, “InGaAs–AlInAs/InP terahertz quantum cascade laser”, *Applied Physics Letters,* vol. 87, pp. 141107-1 - 141107-3, 2005, DOI: 10.1063/1.2081122

25. M. S. Leite, R. L. Woo, W. D. Hong, D. C. Law, and H. A. Atwater, “InAlAs epitaxial growth for wide band gap solar cells” in *IEEE Proceedings of 37th Photovoltaic Specialists Conference,* pp. 780-783, Seattle, USA, 2011.

26. M. S. Leite, R. L. Woo, W. D. Hong, D. C. Law, and H. A. Atwater, “Wide-band-gap InAlAs solar cell for an alternative multijunction approach”, *Applied Physics Letters,* vol. 98, pp. 093502-1 - 093502-3, 2011, DOI: 10.1063/1.3531756

27. ECEn IMMERSE Web Team, Brigham Young University. (2009) Energy Gap in III-V Ternary Semiconductors. [Online]. Available: http://www.cleanroom.byu.edu/EW_ternary.phtml

28. Ioffe Physical Technical Institute. (2005) NSM Archive - Physical Properties of Semiconductors. [Online]. Available: http://www.ioffe.ru/SVA/NSM/Semicond/

29. Harish Palaniappan. (2012) Solar Cells. [Online]. Available: http://solar_cells.tripod.com/notes_sel_1.html

30. Stuart Bowden. (2010) Energy of a Photon | pveducation.org. [Online]. Available: http://www.pveducation.org/pvcdrom/properties-of-sunlight/energy-of-photon

31. J. G. Fossum, “Physical operation of back-surface-field silicon solar cells,” *IEEE Transactions on Electron Devices,* vol. 24, no. 4, pp. 322-325, Apr. 1977.

32. L. Knuuttila, K. Kainu, M. Sopanen, and H. Lipsanen, “In(Ga)As quantum dots on Ge substrate,” *Journal of Materials Science: Materials in Electronics,* vol. 14, no. 5, pp. 349-352, 2003.

33. Ming-Chun Tseng, Ray-Hua Horng, Fan-Lei Wu, Snin-Nan Lin, Hsin Her Yu, and Dong-Sing Wuu, “Crystalline quality and photovoltaic performance of InGaAs solar cells grown on GaAs substrate with large-misoriented angle,” *Vacuum,* vol. 86, no. 7, pp. 843-847, Feb. 2012.

34. Md. Sharafat Hossain, Nowshad Amin, M. A. Matin, M. Mannir Aliyu, Takhir Razykov, and Kamaruzzaman Sopian, “A numerical study on the prospects of high efficiency ultra thin $Zn_xCd_{1-x}S$/ CdTe solar cell,” *Chalcogenide Letters,* vol. 8, no. 3, pp. 263-272, Mar. 2011.

35. Lin Aiguo, Ding Jianning, Yuan Ningyi, Wang Shubo, Cheng Guanggui, and Lu Chao, "Analysis of the p^+/p window layer of thin film solar cells by simulation," *Journal of Semiconductors,* vol. 33, no. 2, pp. 023002-1 - 023002-6 , 2012. DOI:10.1088/1674-4926/33/2/023002

36. C. Lee, H. Efstathiadis, J. E. Raynolds, and P. Haldar, "Two-dimensional Computer Modeling of Single Junction a-Si:H Solar Cells", in IEEE *Proceedings of 34th Photovoltaic Specialists Conference,* pp. 1118-1122, Philadelphia, USA, 2009.

37. S. Bothra, and J.M. Borrego, "Design of GaAs solar cells with low doped base," *Solar Cells,* vol. 28, no. 1, pp. 95-102, Jan. 1990.

38. N. Bouarissa, and M. Boucenna, "Band parameters for AlAs, InAs and their ternary mixed crystals", *Physica Scripta,* vol. 79, pp. 015701-1 - 015701-7 , 2009, DOI: 10.1088/0031-8949/79/01/015701

39. K. H. Goetz, D. Bimberg, H. Jurgensen, J. Selders, A.V.Solomonov, G.F.Glinskii, and M. Razeghi, "Optical and crystallographic properties and impurity incorporation of $Ga_xIn_{1-x}As$ ($0.44<x<0.49$) grown by liquid phase epitaxy, vapor phase epitaxy, and metal organic chemical vapor deposition", *Journal of Applied Physics,* vol. 54, no.8, pp.4543-4552, 1983.

40. J.W. Matthews, and A.E. Blakeslee, "Defects in epitaxial multilayers: I. Misfit dislocations", *Journal of Crystal Growth,* vol. 27, pp. 118- 125, 1974.

41. H. J. Scheel, P. Capper, *Crystal Growth Technology: From Fundamentals and Simulation to Large-scale Production,* p. 307, Wiley-VCH Verlag GmbH & Co. KGaA, Weinheim, Germany, 2008, ISBN: 978-3527317622

42. E. Popova, J. Faure-Vincent, C. Tiusan, C. Bellouard, H. Fischer, M. Hehn, F. Montaigne, M. Alnot, S. Andrieu, and A. Schuhl, "Epitaxial MgO layer for low-resistance and coupling-free magnetic tunnel junctions", *Applied Physics Letters,* vol. 81, no. 6, pp. 1035-1037, 2002.

43. P. K. Nayak, G. G. Belmonte, A. Kahn, J. Bisquert, and D. Cahen, "Photovoltaic efficiency limits and material disorder", *Energy and Environmental Science,* 2012, vol. 5, pp. 6022-6039, DOI: 10.1039/c2ee03178g

44. K. Van Nieuwenhuysen, F. Duerinckx, I. Kuzma, D. van Gestel, G. Beaucarne, J. Poortmans, "Progress in epitaxial deposition on low-cost substrates for thin-film crystalline silicon solar cells at IMEC", *Journal of Crystal Growth,* vol. 287, pp. 438–441, 2006.

45. P. P. Boix, M.M.Wienk, R. A. J. Janssen, and G.Garcia-Belmonte, "Open-Circuit Voltage Limitation in Low-Bandgap Diketopyrrolopyrrole-Based Polymer Solar Cells Processed from Different Solvents", Journal of Physical Chemistry C, vol. 115, pp. 15075–15080, 2011.

46. Q. Diduck, and M. Margala, "Ballistic deflection transistor and logic circuits based on same", U.S. Patent 7576353, Aug. 18, 2009.

47. E. W. Kiewra, S. J. Koester, D. K. Sadana, G. Shahldi, and Y. Sun, "Buried channel MOSFET using III-V compound semiconductors and high k gate dielectrics", US Patent App. Pub. No. US2008/ 0296622 A1, Dec. 2008.

48. L. P. Sadwick, C. W. Kim, K. L. Tan, and D. C. Streit, "Schottky barrier heights of n-type and p-type $Al_{0.48}In_{0.52}As$", *IEEE Electron Device Letters,* vol. 12, pp. 626-628, Nov. 1991.

49. A.W. Bett , F. Dimroth , G. Stollwerck, and O.V. Sulima, "III-V compounds for solar cell applications", Applied Physics A, vol. 69, pp. 119–129, 1999, DOI: 10.1007/s003399900062

50. T. H. Glisson, J. R. Hauser, M. A. Littlejohn, and C. K. Williams, “Energy bandgap and lattice constant contours of III-V quaternary alloys”, Journal of Electronic Materials, vol. 7, no. 1, pp. 1-16, 1978.